Journal of Computational Physics 228 (2009) 236–256

Contents lists available at ScienceDirect

Journal of Computational Physics

journal homepage: www.elsevier.com/locate/jcp

Non-negativity and stability analyses of lattice Boltzmann method for advection–diffusion equation

Borja Servan-Camas [1], Frank T.-C. Tsai *

Department of Civil and Environmental Engineering, Louisiana State University, 3418G Patrick F. Taylor Hall, Baton Rouge, LA 70803-6405, United States

ARTICLE INFO

Article history:
Received 30 April 2007
Received in revised form 2 July 2008
Accepted 8 September 2008
Available online 13 September 2008

Keywords:
Lattice Boltzmann equation
Stability
BGK
Mass transport

ABSTRACT

Stability is one of the main concerns in the lattice Boltzmann method (LBM). The objectives of this study are to investigate the linear stability of the lattice Boltzmann equation with the Bhatnagar–Gross–Krook collision operator (LBGK) for the advection–diffusion equation (ADE), and to understand the relationship between the stability of the LBGK and non-negativity of the equilibrium distribution functions (EDFs). This study conducted linear stability analysis on the LBGK, whose stability depends on the lattice Peclet number, the Courant number, the single relaxation time, and the flow direction. The von Neumann analysis was applied to delineate the stability domains by systematically varying these parameters. Moreover, the dimensionless EDFs were analyzed to identify the non-negative domains of the dimensionless EDFs. As a result, this study obtained linear stability and non-negativity domains for three different lattices with linear and second-order EDFs. It was found that the second-order EDFs have larger stability and non-negativity domains than the linear EDFs and outperform linear EDFs in terms of stability and numerical dispersion. Furthermore, the non-negativity of the EDFs is a sufficient condition for linear stability and becomes a necessary condition when the relaxation time is very close to 0.5. The stability and non-negativity domains provide useful information to guide the selection of dimensionless parameters to obtain stable LBM solutions. We use mass transport problems to demonstrate the consistency between the theoretical findings and LBM solutions.

1. Introduction

The lattice Boltzmann method (LBM) is a mesoscopic numerical method that simulates macroscopic fluid dynamics based on mesoscopic kinetic equations [1]. Developed as an improvement of the lattice gas automata (LGA) [2], the LBM has received great attention not only in hydrodynamic problems, but also in mass transport problems, e.g. the reaction–diffusion equation [3], the contaminant transport equation [4], and coupled density-dependent flow and heat/mass transfer problem [5,6]. Most studies using the LBM have focused on the lattice Boltzmann equation with the Bhatnagar–Gross–Krook collision operator [7] (LBGK), and this will be the focus of our study.

The numerical stability of the LBM still remains a challenge because it involves linear and non-linear stability. While the linear stability analysis might be sufficient to analyze stability when hydrodynamic gradients are weak, it is not sufficient in the general case where hydrodynamic gradients can lead to non-linear instabilities.

One of the earliest works that investigated the stability problem in the LBM was provided by Sterling and Chen [8], where the LBGK was linearized for the fluctuating quantities of particle distribution functions with respect to the equilibrium

* Corresponding author. Tel.: +1 225 578 4246; fax: +1 225 578 4945.
E-mail addresses: bserva1@lsu.edu (B. Servan-Camas), ftsai@lsu.edu (F.T.-C. Tsai).
[1] Tel.: +1 225 620 3296; fax: +1 225 578 4945.

0021-9991/$ - see front matter © 2008 Elsevier Inc. All rights reserved.
doi:10.1016/j.jcp.2008.09.005

distribution functions (EDFs). The von Neumann analysis was carried out to identify the most unstable directions and wave numbers, and their relationship with the mean flow field, relaxation time, and mass distribution parameters. Worthing et al. [9] extended the work of Sterling and Chen [8] to non-uniform flows. In particular, the case of a shear background flow was studied and some stability boundaries were found.

In order to improve the stability of the LBM, several approaches have been introduced. The entropic LBM (ELBM) considers that the instability arises from violating the second law of thermodynamics. Therefore, inclusion of the H theorem in the LBM was suggested to ensure positive production of entropy [10,11]. The equilibrium state in the ELBM is not explicitly needed since the collision integral can be formulated based on knowledge of the H function [12]. To ensure the implementation of the H theorem, one must first find the kinetic state after collision that does not increase entropy during the collision process, and this kinetic state fixes a limit for the new state after the collision. The ELBM provides unconditional stability [13], but was computationally expensive because the isentropic state must be obtained by solving a non-linear equation at each lattice and at every time step [14]. In Chikatamarla et al. [15], an analytical solution to the collision step was found, improving the efficiency of the ELBM.

Comparisons between the LBGK and ELBM show that the ELBM is more stable and allows increasing the Reynolds number [16]. Despite the increase of stability, the ELBM still suffers from spurious oscillations in regions with strong hydrodynamic gradients, such as shock waves [17]. However, a great reduction of the spurious oscillations in the ELBM can be achieved by selecting proper lattice velocities to retain complete Galilean invariance [18].

Improving stability can also be achieved by enforcing the non-negativity of particle distributions. Li et al. [19] introduced a FIX-UP method, which consist of increasing the relaxation time in the LBGK to the minimum value that ensured non-negativity of all particle distribution functions after the collision. Tosi et al. [20] compared the stability behavior of the ELBM and FIX-UP methods with the traditional LBGK, and both methods showed improved stability. While the computational cost is double for the ELBM with respect to the FIX-UP method in one single time step, the ELBM allows increasing the Reynolds number by about an order of magnitude, which makes the ELBM more suitable for high Reynolds number flows.

Brownlee et al. [21] introduced the idea of Enrenfests' steps, in which artificial viscosity is added by returning the particle distributions to their equilibrium states in those points where the variation of entropy between the kinetic state after the collision and the equilibrium state is superior to some threshold. This idea evolved to the concept of the entropy limiters [22], where the particles are smoothly relaxed to their equilibrium based on deviations of entropy from the equilibrium considering also the entropy deviation at the neighbor nodes.

The multi-relaxation times (MRT) method has also shown improvement on the stability of the LBM [23,24]. The main difference of the MRT over the LBGK is that all the particle distributions are not relaxed to the equilibrium state at the same rate. A particular case of MRT is the two relaxation times (TRT), which has been applied to solve mass transport equations and is capable of reducing numerical instabilities [25].

In this work, we focus on the stability of the LBM when solving the advection–diffusion equation (ADE). To our knowledge, the stability problem of using the LBGK to solve the ADE has not been fully discussed, and the aforementioned methods have mainly focused on hydrodynamics equations. To date, no clear stability boundaries have been provided for the LBGK when solving the ADE.

In this study, we carry out linear stability analysis of the LBGK and investigate the relationship between the stability of LBGK and the non-negativity of EDFs since some studies have reported that negative values of the EDFs could quickly lead to numerical instability [26,27]. Linear stability analysis is suitable and can provide insightful information when the hydrodynamic gradients are weak and the flow varies slowly in time (e.g. flows in porous media). Suga [28] carried out linear stability analysis on the LBGK for the ADE, and delineated stability boundaries for several two-dimensional lattices. However, only linear EDFs were considered and the ratio between the lattice speed and the speed of sound was constrained to a specific value, which creates a dependency among the lattice Peclet number, the Courant number, and the relaxation time. In this study, we eliminate this constraint and investigate the linear stability analysis and non-negativity of EDFs in three different lattices. We found that it is crucial for the linear stability and non-negativity analyses to identify the dimensionless parameters locally governing the LBGK.

The rest of this paper is organized as follows: Section 2 formulates the dimensionless EDFs in terms of a scaled Peclet number, Courant number, relaxation time, and flow direction. Section 3 derives non-negative domains for three different lattices and two types of EDFs. Section 4 introduces the linear stability analysis of the LBGK. Section 5 implements the linear stability analysis on the LBGK to delineate stability domains and compares them to the non-negative domains. Section 6 implements numerical examples to validate the stability and non-negativity domains found in Section 5. Section 7 concludes this study.

2. Dimensionless analysis in LBM

2.1. LBM with Bhatnagar–Gross–Krook (BGK) collision operator

The LBM was first developed to solve the equations of hydrodynamics based on the kinetic theory of gases described by the Boltzmann equation. The discrete Boltzmann equation for describing dynamics of local particle distribution functions in a discrete velocity field is

$$\frac{\partial f_i}{\partial t} + \mathbf{c}_i \cdot \nabla f_i = \Omega_i \tag{1}$$

where $f_i(\mathbf{x},t)$ is the particle distribution function moving along the i direction at position $\mathbf{x}$ and time t, $\mathbf{c}_i$ is the streaming velocity along the direction, and Ω_i is the change due to the particle collision. Each direction represents a characteristic direction for the corresponding particle distribution function. In each time step, the particle distribution functions arrive at their neighboring nodes at the same time through prescribed lattice connections. Therefore, the streaming velocity $\mathbf{c}_i$ along the i direction is not arbitrary and is determined by the lattice connection and size. The lattice Boltzmann equation is obtained by integrating Eq. (1) in time along the i direction. This yields [29]

$$f_i(\mathbf{x}, t + \Delta t) = f_i(\mathbf{x} - \mathbf{c}_i \Delta t, t) + \Delta t \Omega_i \tag{2}$$

where Δt is the time step. The BGK collision operator is [7]

$$\Delta t \Omega_i = -\frac{1}{\tau}\left(f_i(\mathbf{x} - \mathbf{c}_i \Delta t, t) - f_i^{\mathrm{eq}}(\mathbf{x}, t + \Delta t)\right) \tag{3}$$

where τ is the single relaxation time and f_i^{eq} are the equilibrium distribution functions (EDFs). Therefore, the LBGK becomes

$$f_i(\mathbf{x}, t + \Delta t) = f_i(\mathbf{x} - \mathbf{c}_i \Delta t, t) - \frac{1}{\tau}\left(f_i(\mathbf{x} - \mathbf{c}_i \Delta t, t) - f_i^{\mathrm{eq}}(\mathbf{x}, t + \Delta t)\right). \tag{4}$$

Eq. (4) represents the evolution of the particle distribution functions through the streaming and collision steps, where conservations of physical quantities at lattice nodes must be satisfied. A general expression of the EDFs f_i^{eq} up to the second-order can be obtained using the Ansatz method as follows [26]:

$$f_i^{\mathrm{eq}} = \rho \omega_i (B_{i0} + B_{i1}\mathbf{u} \cdot \mathbf{c}_i + B_{i2}(\mathbf{u} \cdot \mathbf{c}_i)^2 + B_{i3}(\mathbf{u} \cdot \mathbf{u})) \tag{5}$$

where ω_i, B_{i0}, B_{i1}, B_{i2}, and B_{i3} are obtained by imposing lattice symmetries, and the following constraints for the zero, first, and second moments of EDFs in the phase space

$$\sum_i f_i^{\mathrm{eq}} = \rho \tag{6}$$

$$\sum_i f_i^{\mathrm{eq}} c_{i\xi} = \rho u_\xi \tag{7}$$

$$\sum_i f_i^{\mathrm{eq}} c_{i\xi} c_{i\eta} = \rho(\delta_{\xi\eta} c_S^2 + u_\xi u_\eta) \tag{8}$$

where ξ and η represent the Cartesian indexes, $\delta_{\xi\eta}$ is the Kronecker delta, c_S is the numerical speed of sound when solving hydrodynamics and a numerical parameter related to the diffusion coefficient when solving the advection–diffusion equation (ADE), $\mathbf{u}$ represents flow velocity, and ρ represents density in the hydrodynamic problem and concentration in the mass transport problem. The expressions for the EDFs are given by

$$f_i^{\mathrm{eq}} = \rho \omega_i \left(\frac{c_S^2}{c^2} + \frac{\mathbf{u} \cdot \mathbf{c}_i}{c^2} + \frac{3}{2}\frac{(\mathbf{u} \cdot \mathbf{c}_i)^2}{c^4} - \frac{1}{2}\frac{\mathbf{u} \cdot \mathbf{u}}{c^2}\right) \quad i > 0 \tag{9}$$

$$f_0^{\mathrm{eq}} = \rho - \sum_{i>0} f_i^{\mathrm{eq}} \tag{10}$$

where $c = \Delta x/\Delta t$ is the lattice speed, and ω_i are the weighting factors that depend on lattice directions and the type of lattice to be used. Fig. 1 shows an example of a two-dimensional lattice with nine directions (D2Q9). Eq. (9) can also be derived as a Taylor expansion of the Maxwell–Boltzmann distribution up to second-order in the Mach number [1] or as a Taylor expansion up to second-order in Mach number around the kinetic states that minimize an H function [11].

2.2. Dimensionless equilibrium distribution functions

For the purpose of convenience, we introduce dimensionless EDFs, defined as $g_i^{\mathrm{eq}} = f_i^{\mathrm{eq}}/\rho$. Let $\mathbf{e}_i = \mathbf{c}_i/c$ and $\mathbf{e}_{\mathbf{u}} = \mathbf{u}/|\mathbf{u}|$, where $\mathbf{e}_{\mathbf{u}}$ is the unit vector along the direction of the macroscopic velocity, and $\mathbf{e}_0 = \mathbf{0}$. The angle $\alpha = \arccos(\mathbf{e}_{\mathbf{u}} \cdot \mathbf{e}_1)$ is defined as the angle of the flow velocity with respect to the lattice grid in two dimensions, and is shown in Fig. 1. Using $\mathbf{e}_i$ and $\mathbf{e}_{\mathbf{u}}$ in Eq. (9), the dimensionless EDFs become

$$g_i^{\mathrm{eq}} = \omega_i \left(\frac{c_S^2}{c^2} + \frac{|\mathbf{u}|}{c}(\mathbf{e}_i \cdot \mathbf{e}_{\mathbf{u}}) + \frac{|\mathbf{u}|^2}{c^2}\left(\frac{3}{2}(\mathbf{e}_i \cdot \mathbf{e}_{\mathbf{u}})^2 - \frac{1}{2}\right)\right) \quad i > 0 \tag{11}$$

$$g_0^{\mathrm{eq}} = 1 - \sum_{i>0} g_i^{\mathrm{eq}} \tag{12}$$

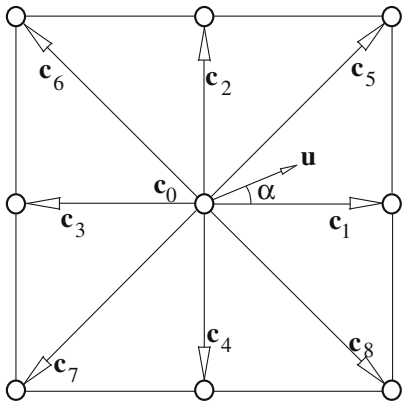

Fig. 1. D2Q9 lattice and flow direction.

The diffusion coefficient D is recovered in the LBM as follows:

$$D = c_S^2 \Delta t \left(\tau - \frac{1}{2}\right) \tag{13}$$

Eq. (13) is the same as in Flekkøy [30] when considering lattice units ($\Delta x = 1$ and $\Delta t = 1$) and $c/c_S = \sqrt{3}$. However, the constraint $c/c_S = \sqrt{3}$ is not necessary for the mass transport problem.

This study focuses on the non-negativity of the dimensionless EDFs and the linear stability of the LBGK applied to the ADE. Therefore, the lattice Peclet number $Pe_{\Delta x} = |\mathbf{u}|\Delta x/D$ and the Courant number $Cr = |\mathbf{u}|/c = |\mathbf{u}|\Delta t/\Delta x$ are introduced into Eq. (11). Substituting the lattice Peclet number, the Courant number, and Eq. (13) into Eq. (11), the dimensionless EDFs become

$$g_i^{\mathrm{eq}} = \omega_i \left(\frac{Cr}{Pe_{\Delta x}(\tau - 1/2)} + Cr(\mathbf{e_u} \cdot \mathbf{e}_i) + Cr^2 \left(\frac{3}{2}(\mathbf{e_u} \cdot \mathbf{e}_i)^2 - \frac{1}{2} \right) \right) \quad i > 0 \tag{14}$$

According to Eq. (14), the non-negativity of g_i^{eq} is explicitly influenced by four dimensionless parameters: the lattice Peclet number, the Courant number, the relaxation time, and the flow direction, denoted as ($Pe_{\Delta x}$,Cr,τ,α). Moreover, we introduce the scaled Peclet number, defined as $Pe^*_{\Delta x} = Pe_{\Delta x}(\tau - 1/2)$ to consider the product effect of the lattice Peclet number and the relaxation time. Using $Pe^*_{\Delta x}$ instead of $Pe_{\Delta x}$ allows us to explicitly find the minimum value of the relaxation time that ensures stable solutions for given values of $Pe^*_{\Delta x}$, Cr, and α in the later linear stability analysis. Introducing $Pe^*_{\Delta x} = Pe_{\Delta x}(\tau - 1/2)$ into Eq. (14), we obtain

$$g_i^{\mathrm{eq}} = \omega_i \left(\frac{Cr}{Pe^*_{\Delta x}} + Cr(\mathbf{e_u} \cdot \mathbf{e}_i) + Cr^2 \left(\frac{3}{2}(\mathbf{e_u} \cdot \mathbf{e}_i)^2 - \frac{1}{2} \right) \right) \quad i > 0 \tag{15}$$

In short, the non-negativity and stability analyses will be based on the parameter space $\prod = (Pe^*_{\Delta x}, Cr, \tau, \alpha)$ for the ADE.

If solving the hydrodynamics equations, the following relationship between the kinematic viscosity and the numerical parameters of the LBM holds [1]

$$v = \frac{c^2}{3} \Delta t \left(\tau - \frac{1}{2} \right) \tag{16}$$

where v is the kinematic viscosity of the fluid. It is convenient to use the lattice Reynolds number $Re_{\Delta x} = |\mathbf{u}|\Delta x/v$ and the Mach number $M = |\mathbf{u}|/c_S$ to analyze the dimensionless EDFs

$$g_i^{\mathrm{eq}} = \omega_i \left(\frac{(\tau - 1/2)^2}{9} \frac{Re^2_{\Delta x}}{M^2} + \frac{(\tau - 1/2)}{3} Re_{\Delta x}(\mathbf{e_u} \cdot \mathbf{e}_i) + \frac{(\tau - 1/2)^2}{9} Re^2_{\Delta x} \left(\frac{3}{2}(\mathbf{e_u} \cdot \mathbf{e}_i)^2 - \frac{1}{2} \right) \right) \quad i > 0. \tag{17}$$

In this case, the dimensionless EDFs are governed by four parameters: the lattice Reynolds number, the Mach number, the relaxation time, and the flow direction, denoted as ($Re_{\Delta x}$,M,τ,α). For the purpose of the stability analysis, we can also use the scaled Reynolds number $Re^*_{\Delta x} = Re_{\Delta x}(\tau - 1/2)$ to find the minimum value of the relaxation time to derive stable solutions for given values of $Re^*_{\Delta x}$, M, and α. Using the scaled Reynolds number, Eq. (17) becomes

$$g_i^{\mathrm{eq}} = \omega_i \left(\frac{{Re^*_{\Delta x}}^2}{9M^2} + \frac{Re^*_{\Delta x}}{3}(\mathbf{e_u} \cdot \mathbf{e}_i) + \frac{{Re^*_{\Delta x}}^2}{9} \left(\frac{3}{2}(\mathbf{e_u} \cdot \mathbf{e}_i)^2 - \frac{1}{2} \right) \right) \quad i > 0 \tag{18}$$

Given the four parameters, $\prod = (Re^*_{\Delta x}, M, \tau, \alpha)$, the non-negativity of g_i^{eq} and the stability of the LBGK can be determined.

Eq. (11) provides a general form of the dimensionless EDFs that can be used to perform non-negative and stability analyses for both hydrodynamic and mass transport problems. In other words, once the non-negativity and linear stability analyses are carried out for the ADE using Eq. (15), the stability set for $\prod = (Pe^*_{\Delta x}, Cr, \tau, \alpha)$ can be transformed into the stability set $\prod = (Re^*_{\Delta x}, M, \tau, \alpha)$ through the following relationships:

$$Re^*_{\Delta x} = 3Cr \tag{19}$$

$$M^2 = CrPe^*_{\Delta x} \tag{20}$$

Since this work focuses on the non-negativity and stability analyses of the ADE and therefore, we will use the parameter space given by $\prod = (Pe^*_{\Delta x}, Cr, \tau, \alpha)$.

3. Non-negativity analysis of equilibrium distribution functions

This section analyzes the sufficient conditions in terms of $Pe^*_{\Delta x}$ and Cr for obtaining non-negative values of the second-order EDFs in a D2Q9 lattice given by Eqs. (12) and (15) for any directions of the macroscopic velocity $\mathbf{u}$. Let S^{D2Q9}_{NL} be the set of $(Pe^*_{\Delta x}, Cr)$ that is conditioned on the non-negativity of second-order EDFs for any flow directions:

$$S^{D2Q9}_{NL} = \left\{(Pe^*_{\Delta x}, Cr) | Pe^*_{\Delta x} > 0, Cr > 0,\ \forall\ \alpha \in [0, 2\pi],\ \forall\ i : g^{eq}_i(Pe^*_{\Delta x}, Cr) \geqslant 0\right\} \tag{21}$$

where α is the angle between $\mathbf{u}$ and $\mathbf{c}_1$ shown in Fig. 1. Due to the symmetry of the lattice directions, we can reduce our analysis to the range $\alpha \in [0, \pi/4]$. Any flow direction will give the same result for an angle in $[0,\pi/4]$ after reordering the lattice velocities $\mathbf{c}_i$. Therefore, Eq. (21) is rewritten as

$$S^{D2Q9}_{NL} = \left\{(Pe^*_{\Delta x}, Cr) | Pe^*_{\Delta x} > 0,\ Cr > 0,\ \forall\ \alpha \in [0, \pi/4],\ \forall i :\ g^{eq}_i(Pe^*_{\Delta x}, Cr) \geqslant 0\right\}. \tag{22}$$

Consider the set of $(Pe^*_{\Delta x}, Cr)$ from individual non-negative EDFs:

$$S_i = \left\{(Pe^*_{\Delta x}, Cr) | Pe^*_{\Delta x} > 0,\ Cr > 0,\ \forall\ \alpha \in [0, \pi/4],\ g^{eq}_i(Pe^*_{\Delta x}, Cr) \geqslant 0\right\}. \tag{23}$$

Eq. (22) represents the intersection of all S_i, i.e., $S = \bigcap_{i=0}^{8} S_i$. For D2Q9, we have $\mathbf{e}_i = \cos(\beta_i), \sin(\beta_i))$ with $\beta_i = (i-1)\pi/2$ for $i = 1,2,3,4$, and $\mathbf{e}_i = \sqrt{2}(\cos(\beta_i), \sin(\beta_i))$ with $\beta_i = \pi/4 + (i-5)\pi/2$ for $i = 5,6,7,8$, and $\mathbf{e_u} = (\cos(\alpha), \sin(\alpha))$ Inserting $\mathbf{e}_i \cdot \mathbf{e_u}$ into Eq. (15), we obtain the dimensionless EDFs for a given flow direction α:

$$g^{eq}_1 = \frac{1}{3}\left(\frac{Cr}{Pe^*_{\Delta x}} + Cr\cos\alpha + Cr^2\left(\frac{3}{2}\cos^2\alpha - \frac{1}{2}\right)\right) \tag{24}$$

$$g^{eq}_2 = \frac{1}{3}\left(\frac{Cr}{Pe^*_{\Delta x}} + Cr\sin\alpha + Cr^2\left(\frac{3}{2}\sin^2\alpha - \frac{1}{2}\right)\right) \tag{25}$$

$$g^{eq}_3 = \frac{1}{3}\left(\frac{Cr}{Pe^*_{\Delta x}} - Cr\cos\alpha + Cr^2\left(\frac{3}{2}\cos^2\alpha - \frac{1}{2}\right)\right) \tag{26}$$

$$g^{eq}_4 = \frac{1}{3}\left(\frac{Cr}{Pe^*_{\Delta x}} - Cr\sin\alpha + Cr^2\left(\frac{3}{2}\sin^2\alpha - \frac{1}{2}\right)\right) \tag{27}$$

$$g^{eq}_5 = \frac{1}{12}\left(\frac{Cr}{Pe^*_{\Delta x}} + Cr(\cos\alpha + \sin\alpha) + Cr^2\left(\frac{3}{2}(\cos\alpha + \sin\alpha)^2 - \frac{1}{2}\right)\right) \tag{28}$$

$$g^{eq}_6 = \frac{1}{12}\left(\frac{Cr}{Pe^*_{\Delta x}} + Cr(-\cos\alpha + \sin\alpha) + Cr^2\left(\frac{3}{2}(-\cos\alpha + \sin\alpha)^2 - \frac{1}{2}\right)\right) \tag{29}$$

$$g^{eq}_7 = \frac{1}{12}\left(\frac{Cr}{Pe^*_{\Delta x}} - Cr(\cos\alpha + \sin\alpha) + Cr^2\left(\frac{3}{2}(\cos\alpha + \sin\alpha)^2 - \frac{1}{2}\right)\right) \tag{30}$$

$$g^{eq}_8 = \frac{1}{12}\left(\frac{Cr}{Pe^*_{\Delta x}} + Cr(\cos\alpha - \sin\alpha) + Cr^2\left(\frac{3}{2}(\cos\alpha - \sin\alpha)^2 - \frac{1}{2}\right)\right) \tag{31}$$

Because we only need to study the EDFs with$\alpha \in [0, \pi/4]$, the values $\cos\alpha \in [\sqrt{2}/2, 1]$, $\sin\alpha \in [0, \sqrt{2}/2]$, and $\cos(\alpha) - \sin(\alpha) \in [0, 1]$. Then Eqs. (24)–(31) render the relations: $g^{eq}_1 \geqslant g^{eq}_3$, $g^{eq}_2 \geqslant g^{eq}_4$, $g^{eq}_5 \geqslant g^{eq}_7$, and $g^{eq}_8 \geqslant g^{eq}_6$. Therefore, $S_3 \subset S_1$, $S_4 \subset S_2$, $S_7 \subset S_5$, $S_6 \subset S_8$, and $S = S_0 \cap S_3 \cap S_4 \cap S_6 \cap S_7$. Let S^* be $S_3 \cap S_4 \cap S_6 \cap S_7$. Then $S^{D2Q9}_{NL} = S_0 \cap S_*$.

3.1. Calculation of S_0

By definition, S_0 is the domain where g_0^{eq} is non-negative:

$$S_0 = \left\{(Pe^*_{\Delta x}, Cr) | Pe^*_{\Delta x} > 0, Cr > 0, \quad \forall\ \alpha \in [0, \pi/4],\ g_0^{eq}(Pe^*_{\Delta x}, Cr) \geqslant 0\right\} \tag{32}$$

where for D2Q9, g_0^{eq} is

$$g_0^{eq} = 1 - \frac{5}{3}\frac{Cr}{Pe^*_{\Delta x}} - \frac{2}{3}Cr^2. \tag{33}$$

Then, $g_0 \geqslant 0$ if and only if $3Pe^*_{\Delta x} - 5Cr - 2Cr^2 Pe^*_{\Delta x} \geqslant 0$ and

$$S_0 = \left\{(Pe^*_{\Delta x}, Cr) | Pe^*_{\Delta x} > 0,\ Cr > 0,\ 3Pe^*_{\Delta x} - 5Cr - 2Cr^2 Pe^*_{\Delta x} \geqslant 0\right\}. \tag{34}$$

3.2. Calculation of S^*

Since the weighting factors ω_i are positive by definition, for $\forall \alpha \in [0, \pi/4]$ the set S^* can be redefined as

$$S_* = \left\{(Pe^*_{\Delta x}, Cr) | Pe^*_{\Delta x} > 0,\ Cr > 0,\ \frac{Cr}{Pe^*_{\Delta x}} - Cr\lambda_i + Cr^2\left(\frac{3}{2}\lambda_i^2 - \frac{1}{2}\right) \geqslant 0,\ i = 3, 4, 6, 7\right\} \tag{35}$$

where $\lambda_i = \mathbf{e}_i \cdot \mathbf{e_u}$. Hence, $\lambda_3 = \cos\alpha$, $\lambda_4 = \sin\alpha$, $\lambda_6 = \cos\alpha - \sin\alpha$, and $\lambda_7 = \cos\alpha + \sin\alpha$. Because $\alpha \in [0, \pi/4]$, we have $\lambda_3 \in [\sqrt{2}/2, 1]$, $\lambda_4 \in [0, \sqrt{2}/2]$, $\lambda_6 \in [0, 1]$, and $\lambda_7 \in [1, \sqrt{2}]$. Therefore, S^* becomes

$$S_* = \left\{(Pe^*_{\Delta x}, Cr) | Pe^*_{\Delta x} > 0,\ Cr > 0, \quad \forall \lambda \in [0, \sqrt{2}] : h(Pe^*_{\Delta x}, Cr, \lambda) \geqslant 0\right\} \tag{36}$$

where $h(Pe^*_{\Delta x}, Cr, \lambda) = Cr/Pe^*_{\Delta x} - Cr\lambda + Cr^2(3\lambda^2/2 - 1/2)$. According to Eq. (36), S^* is bounded by the curve $h(Pe^*_{\Delta x}, Cr, \lambda = \sqrt{2}) = 0$ and the envelope of the parametric family of curves $h(Pe^*_{\Delta x}, Cr, \lambda) = 0$ whose parameter is $\lambda \in [0, \sqrt{2}]$. The curve $h(Pe^*_{\Delta x}, Cr, \lambda = \sqrt{2}) = 0$ is defined by the following equation:

$$2 - 2\sqrt{2}Pe^*_{\Delta x} + 5Pe^*_{\Delta x}Cr = 0 \tag{37}$$

To obtain the equation of the envelope, we need to eliminate λ in $h(Pe^*_{\Delta x}, Cr, \lambda) = 0$ via $h_\lambda(Pe^*_{\Delta x}, Cr, \lambda) = \mathrm{d}h/\mathrm{d}\lambda = 0$, which gives the value of $\lambda^* = 1/(3Cr)$. Introducing λ^* into $h(Pe^*_{\Delta x}, Cr, \lambda) = 0$, we obtain the equation of the enveloping curve:

$$Pe^*_{\Delta x} + 3Cr^2 Pe^*_{\Delta x} - 6Cr = 0. \tag{38}$$

The intersection of the envelope curve and $h(Pe^*_{\Delta x}, Cr, \lambda = \sqrt{2}) = 0$ is at $Pe^*_{\Delta x} = 1.202$ and $Cr = 0.233$. Thus, the set S^* is obtained for any $\lambda \in [0, \sqrt{2}]$:

$$S_* = \left\{(Pe^*_{\Delta x}, Cr) \middle| \begin{array}{lll} Pe^*_{\Delta x} > 0, Cr > 0 & & \\ 6Cr - Pe^*_{\Delta x} - 3Cr^2 Pe^*_{\Delta x} \geqslant 0; & \text{if} & Cr > 0.233 \\ 2 - 2\sqrt{2}Pe^*_{\Delta x} + 5Pe^*_{\Delta x}Cr \geqslant 0; & \textit{if} & Cr \leqslant 0.233 \end{array}\right\}. \tag{39}$$

3.3. Calculation of S

From Eqs. (34) and (39), the set S_{NL}^{D2Q9} is obtained as the intersection of S_0 and S^*:

$$S_{NL}^{D2Q9} = \left\{(Pe^*_{\Delta x}, Cr) \middle| \begin{array}{l} Pe^*_{\Delta x} > 0, Cr > 0 \\ 3Pe^*_{\Delta x} - 5Cr - 2Cr^2 Pe^*_{\Delta x} \geqslant 0 \\ 6Cr - Pe^*_{\Delta x} - 3Cr^2 Pe^*_{\Delta x} \geqslant 0; \quad \text{if } Cr > 0.233 \\ 2 - 2\sqrt{2}Pe^*_{\Delta x} + 5Pe^*_{\Delta x}Cr \geqslant 0; \quad \text{if } Cr \leqslant 0.233 \end{array}\right\}. \tag{40}$$

Fig. 2 shows the non-negativity domain for all EDFs regardless of the flow directions. The non-negativity domain is bounded by $g_0^{eq}(Pe^*_{\Delta x}, Cr) = 0$, the envelope of the parametric family of curves $h(Pe^*_{\Delta x}, Cr, \lambda) = 0$ for $\lambda \in [0, \sqrt{2}]$, and the curve $h(Pe^*_{\Delta x}, Cr, \lambda = \sqrt{2}) = 0$. Outside the non-negativity domain S, negative values for at least one dimensionless EDF can be obtained for some specific flow directions. Hence, to be inside the domain S is a sufficient condition for non-negativity.

Using linear EDFs (neglecting the second-order terms in velocity in Eqs. (11), (12)) has been suggested for solving the ADE in some specific cases, such as low Courant number [30] and slowly varying solutions [31]. Hence, we are also interested in investigating the non-negativity and stability when using linear EDFs.

Using the same procedures, the non-negative domains for the D1Q3 lattice with linear and second-order EDFs, and for the D2Q5 and D2Q9 lattices with linear EDFs, are derived in Appendix A. The results are the following:

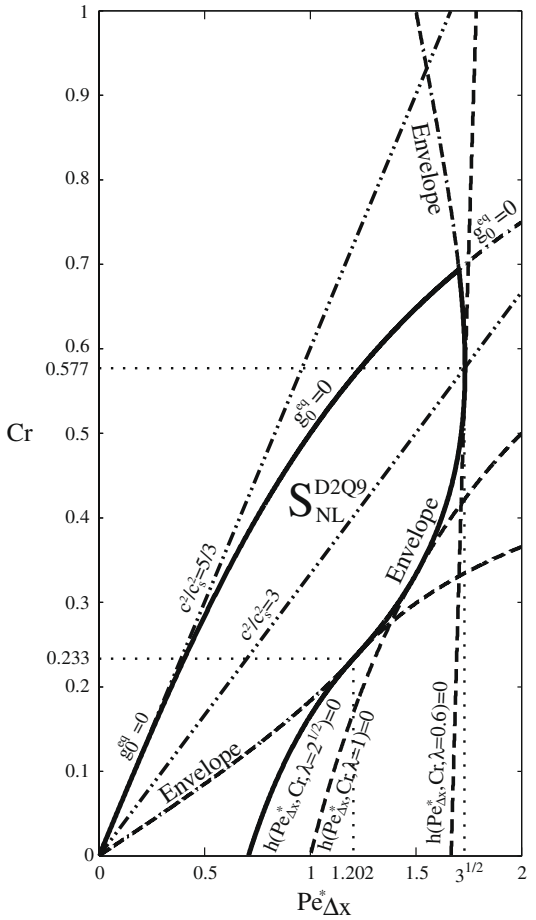

Fig. 2. Non-negativity domain for D2Q9 with second-order EDFs (solid lines).

3.3.1. D1Q3 and linear EDFs

$$S_L^{D1Q3} = \left\{ (Pe^*_{\Delta x}, Cr) \middle| \begin{array}{l} Pe^*_{\Delta x} > 0, Cr > 0 \\ Pe^*_{\Delta x} - Cr \geqslant 0 \\ 1 - Pe^*_{\Delta x} \geqslant 0 \end{array} \right\} \tag{41}$$

3.3.2. D1Q3 and second-order EDFs

$$S_{NL}^{D1Q3} = \left\{ (Pe^*_{\Delta x}, Cr) \middle| \begin{array}{l} Pe^*_{\Delta x} > 0, Cr > 0 \\ Pe^*_{\Delta x} - Cr - Pe^*_{\Delta x} Cr^2 \geqslant 0 \\ 1 - Pe^*_{\Delta x} + Pe^*_{\Delta x} Cr \geqslant 0 \end{array} \right\} \tag{42}$$

3.3.3. D2Q5 and linear EDFs

$$S_L^{D2Q5} = \left\{ (Pe^*_{\Delta x}, Cr) \middle| \begin{array}{l} Pe^*_{\Delta x} > 0, Cr > 0 \\ Pe^*_{\Delta x} - 2Cr \geqslant 0 \\ Pe^*_{\Delta x} \leqslant 1 \end{array} \right\} \tag{43}$$

3.3.4. D2Q9 and linear EDFs

$$S_L^{D2Q9} = \left\{ (Pe^*_{\Delta x}, Cr) \middle| \begin{array}{l} Pe^*_{\Delta x} > 0, Cr > 0 \\ 3Pe^*_{\Delta x} - 5Cr \geqslant 0 \\ Pe^*_{\Delta x} \leqslant \sqrt{2}/2 \end{array} \right\} \tag{44}$$

4. Linear stability analysis of LBGK

In this section, we adopt the von Neumann analysis to study the LBGK (Eq. (4)). Due to the streaming step and mass conservation at the collision step, $\rho(\mathbf{x},t+\Delta t)$ can be written as

$$\rho(\mathbf{x},t+\Delta t)=\sum_j f_j(\mathbf{x}-\mathbf{c}_j\Delta t,t) \tag{45}$$

Introducing $g_i^{eq}(\mathbf{x},t)=f_i^{eq}(\mathbf{x},t)/\rho(\mathbf{x},t)$ and Eq. (45) into Eq. (4), the LBGK becomes

$$f_i(\mathbf{x},t+\Delta t)=\left(1-\frac{1}{\tau}\right)f_i(\mathbf{x}-\mathbf{c}_i\Delta t,t)+\frac{1}{\tau}\left(\sum_j f_j(\mathbf{x}-\mathbf{c}_j\Delta t,t)\right)g_i^{eq}(\mathbf{x},t+\Delta t) \tag{46}$$

In order to analyze the stability of Eq. (46), we consider the dimensionless EDFs to be constant in time and uniform in space such that Eq. (46) becomes a linear system expressing the evolution of the particle distribution functions. Constant and uniform dimensionless EDFs are obtained when the flow field is constant and uniform in the hydrodynamic and mass transport problems. Although this is not the general case, the results of the linear stability analysis can provide fundamental knowledge about the stability of the LBGK.

This approach was used by Suga [28] to study linear stability of the LBGK. Suga [28] applied the von Neumann analysis to Eq. (46) for different lattices using linear EDFs and keeping a constant ratio between the lattice speed and the speed of sound. Although in the hydrodynamic case this ratio has to be fixed to $\sqrt{3}$, the ratio can vary when solving the ADE. In this study, we allow this speed ratio to be any value, which will introduce an additional degree of freedom.

A discrete Fourier series solution for the particle distribution functions is introduced to perform the von Neumann analysis

$$f_i(\mathbf{x},t)=\sum_m b_{im}(t)\mathrm{e}^{-I\mathbf{k}_m\cdot\mathbf{x}} \tag{47}$$

where I is the complex number, $b_{im}(t)$ represents the amplitude, and $\mathbf{k}_m$ represents the wave number. Introducing the Fourier series solution into Eq. (46), for each wave number

$$b_{im}(t+\Delta t)=\left(1-\frac{1}{\tau}\right)b_{im}(t)\mathrm{e}^{-I\mathbf{k}_m\cdot\mathbf{c}_i t}+\frac{1}{\tau}g_i^{eq}(\mathbf{x}-\mathbf{c}_i\Delta t,t)\sum_j b_{jm}(t)\mathrm{e}^{-I\mathbf{k}_m\cdot\mathbf{c}_j\Delta t}. \tag{48}$$

Eq. (48) can be written in a matrix form as follows:

$$\mathbf{b}(t+\Delta t)=\mathbf{A}\mathbf{b}(t) \tag{49}$$

where $\mathbf{A}=(1-1/\tau)\mathbf{M}+(1/\tau)\mathbf{G}$, $\mathbf{M}$ is a diagonal matrix whose diagonal elements are given by $M_{ii}=\mathrm{e}^{-I\mathbf{k}_m\cdot\mathbf{c}_i\Delta t}$, and the elements of matrix $\mathbf{G}$ are given by $G_{ij}=g_i^{eq}(\mathbf{x}-\mathbf{c}_i\Delta t,t)\mathrm{e}^{-I\mathbf{k}_m\cdot\mathbf{c}_j\Delta t}$. The matrix A reads:

$$\mathbf{A}=\left(1-\frac{1}{\tau}\right)\begin{pmatrix}\mathrm{e}^{-I\mathbf{k}_m\cdot\mathbf{c}_0\Delta t} & 0 & \cdots & 0\\ 0 & \mathrm{e}^{-I\mathbf{k}_m\cdot\mathbf{c}_1\Delta t} & \cdots & 0\\ \cdots & \cdots & \ddots & \cdots\\ 0 & 0 & \cdots & \mathrm{e}^{-I\mathbf{k}_m\cdot\mathbf{c}_{Q-1}\Delta t}\end{pmatrix}+\frac{1}{\tau}\begin{pmatrix}g_0^{eq}\mathrm{e}^{-I\mathbf{k}_m\cdot\mathbf{c}_0\Delta t} & g_0^{eq}\mathrm{e}^{-I\mathbf{k}_m\cdot\mathbf{c}_1\Delta t} & \cdots & g_0^{eq}\mathrm{e}^{-I\mathbf{k}_m\cdot\mathbf{c}_{Q-1}\Delta t}\\ g_1^{eq}\mathrm{e}^{-I\mathbf{k}_m\cdot\mathbf{c}_0\Delta t} & g_1^{eq}\mathrm{e}^{-I\mathbf{k}_m\cdot\mathbf{c}_1\Delta t} & \cdots & g_1^{eq}\mathrm{e}^{-I\mathbf{k}_m\cdot\mathbf{c}_{Q-1}\Delta t}\\ \cdots & \cdots & \ddots & \cdots\\ g_{Q-1}^{eq}\mathrm{e}^{-I\mathbf{k}_m\cdot\mathbf{c}_0\Delta t} & g_{Q-1}^{eq}\mathrm{e}^{-I\mathbf{k}_m\cdot\mathbf{c}_1\Delta t} & \cdots & g_{Q-1}^{eq}\mathrm{e}^{-I\mathbf{k}_m\cdot\mathbf{c}_{Q-1}\Delta t}\end{pmatrix} \tag{50}$$

where Q is the number of lattice velocities.

The matrix $\mathbf{A}$ is the amplification matrix of the linear system in Eq. (49). Therefore, the stability of the system depends on the module of the eigenvalues of matrix $\mathbf{A}$, and the LBGK will be stable as long as the module of all the eigenvalues is less than unity for any wave number $\mathbf{k}_m$.

5. Stability analysis for ADE

5.1. Stability analysis on D1Q3

In this section, the eigenvalue problem is solved for the one-dimensional lattice with three velocities, D1Q3. Since the system has only three velocities ($Q=3$), the matrix $\mathbf{A}$ is a 3 by 3 matrix. The eigenvalues of $\mathbf{A}$ are governed by the three parameters $\prod=(Pe^*_{\Delta x},Cr,\tau)$, and the direction of the flow is given by either $\alpha=0$ or $\alpha=\pi$ in the one-dimensional case. The dimensionless EDFs for D1Q3 are

$$g_1^{eq}=\frac{1}{2}\left(\frac{Cr}{Pe^*_{\Delta x}}+Cr+Cr^2\right),\quad g_2^{eq}=\frac{1}{2}\left(\frac{Cr}{Pe^*_{\Delta x}}-Cr+Cr^2\right),\quad g_0^{eq}=1-\left(\frac{Cr}{Pe^*_{\Delta x}}+Cr^2\right) \tag{51}$$

where g_1^{eq} are the dimensionless EDFs for particles moving in the same direction as the flow, g_2^{eq} is for particles moving in the direction opposite the flow, and g_0^{eq} represents resting particles. Due to the complexity of getting the eigenvalues of the matrix **A** analytically as an explicit function of τ, $Pe^*_{\Delta x}$, and Cr, they are obtained numerically. We use the dimensionless wave number $\beta_n = k_{mx}c_{jx}\Delta t = n2\pi/N$, where n is from 1 to N, and N is the number of β_n used in the analysis. Since the values of the particle distribution functions are real numbers, the eigenvalue problem for $\mathbf{k_m}$ gives the same eigenvalue when solving for $-\mathbf{k_m}$.

In order to determine the stability domain, the number of dimensionless wave numbers used is $N = 36$. The eigenvalue problem is solved twice, once based on the pair$(Pe^*_{\Delta x}, Cr)$ and a second time based on $(Pe_{\Delta x},Cr)$, using a grid of 100 by100 points in each case. We test different values of the relaxation time for $\tau = 0.51$, 0.6, 0.7, 0.8, 0.9, and 1.0.

Fig. 3(a) shows the stability domain in terms of $Pe^*_{\Delta x}$ and Cr for $\tau = 0.7$. We observe that the stability domain is bounded by two stability boundaries (stability boundary 1 and stability boundary 2). Stability boundary 1 corresponds to the condition $g_0^{eq} = 0$. There is no direct relationship between stability boundary 2 and the non-negativity of the dimensionless EDFs. Actually, stability boundary 2 lies in the area where $g_2^{eq} < 0$ for $\tau = 0.7$. Therefore, it can be concluded that negative EDF values do not necessarily lead to instabilities. Fig. 3(b) shows that the stability domain grows with increasing relaxation time and that the stability domain using a given value of relaxation time includes the stability domain found when using smaller values of relaxation time.

The non-negativity domain for D1Q3 with second-order EDFs is also shown in Fig. 3(b), to be compared with the stability domains. The non-negativity domain is bounded by two non-negativity boundaries, $g_0^{eq} = 0$ and $g_2^{eq} = 0$, obtained in Eq. (42).

Fig. 3 presents two important features. First, stability boundary 2 approaches the non-negativity boundary of $g_2^{eq} = 0$ as the relaxation time decreases, and the non-negativity domain becomes the stability domain when the relaxation time is very close to 0.5. Second, if the pair $(Pe^*_{\Delta x}, Cr)$ lies in the stability domain for a given value of the relaxation time, the pair also lies in the stability domain if larger values of the relaxation time are used. In other words, given $Pe^*_{\Delta x}$ and Cr values, there exists a minimum value of the relaxation time τ for stable solutions.

Fig. 4 redraws the stability domains provided by Fig. 3(b) in terms of $Pe_{\Delta x}$ and Cr. Because of the decoupling of the relaxation time from the lattice Peclet number, a larger value of the relaxation time does not necessarily result in stable solutions. This shows the advantage of using $Pe^*_{\Delta x}$ instead of $Pe_{\Delta x}$ for the analysis.

If only the linear terms are considered, the dimensionless EDFs become

$$g_1^{eq} = \frac{1}{2}\left(\frac{Cr}{Pe^*_{\Delta x}} + Cr\right), \quad g_2^{eq} = \frac{1}{2}\left(\frac{Cr}{Pe^*_{\Delta x}} - Cr\right), \quad g_0^{eq} = 1 - \frac{Cr}{Pe^*_{\Delta x}} \tag{52}$$

Fig. 5 shows the stability boundaries for different values of relaxation time for the linear EDFs. The stability domain is bounded by stability boundary 1 and stability boundary 2 for a given relaxation time. Stability boundary 1 is given by $g_0^{eq} = 0$ and stability boundary 2 moves and enlarges the stability domain as the relaxation time increases. Comparing Fig. 5 with Fig. 3(b), we can observe that the stability domains with second-order EDFs are larger than those with linear EDFs

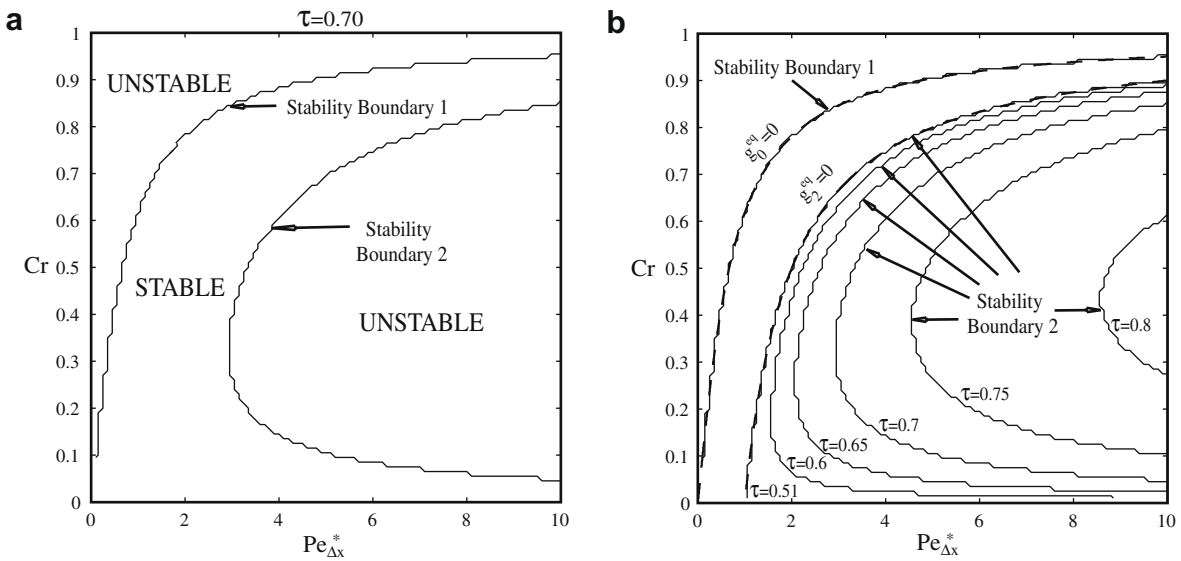

Fig. 3. Linear stability boundaries for LBGK in D1Q3 with second-order EDFs: (a) specific case $\tau = 0.70$; (b) different τ values (solid lines) and non-negativity boundaries (dash lines) for dimensionless EDFs.

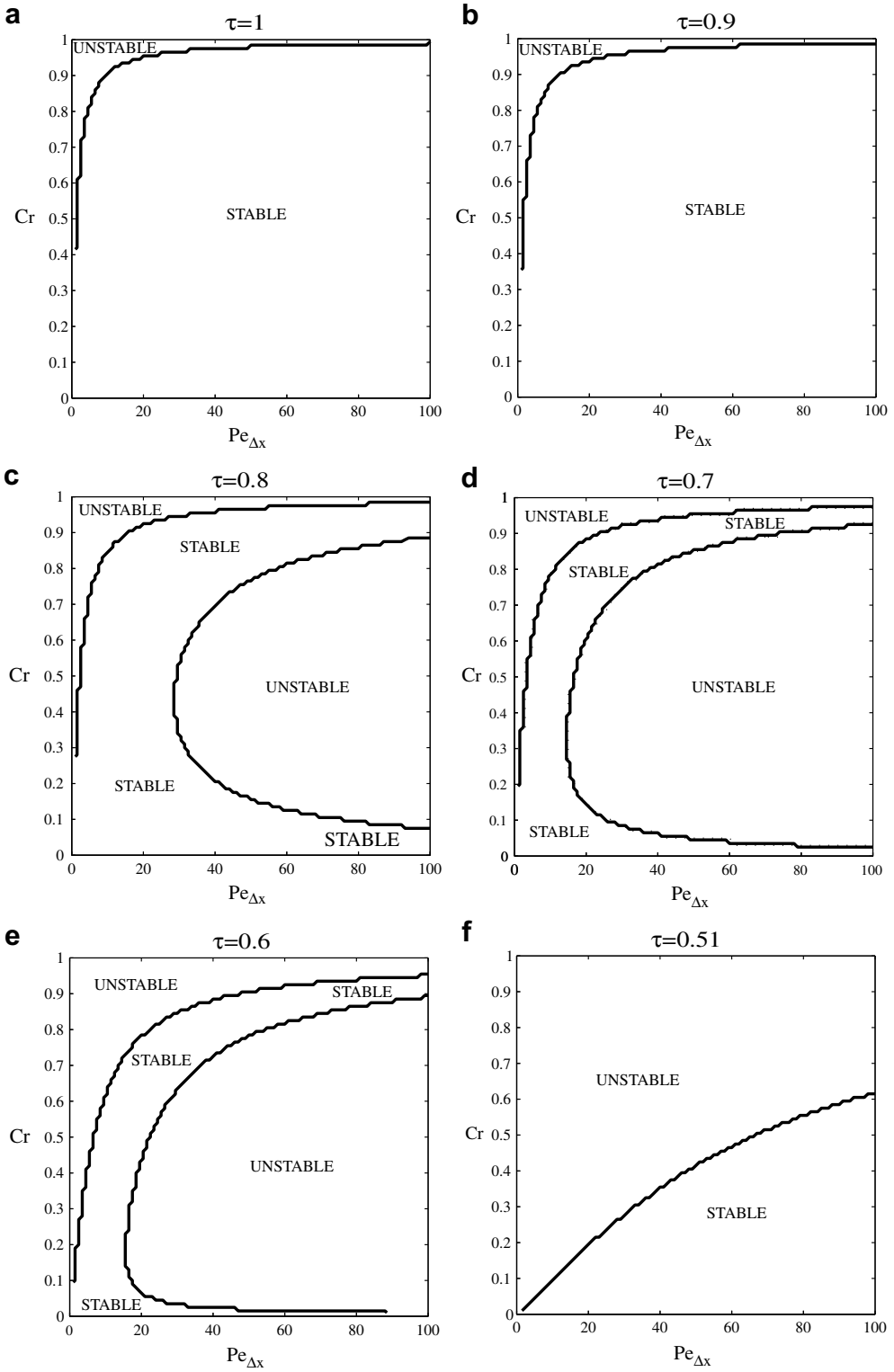

Fig. 4. Linear stability boundaries for LBGK model in D1Q3 with second-order EDFs.

for a given τ. In Karlin et al. [32], non-linear EDFs were also used resulting in more stable realizations. The non-negativity domain with second-order EDFs is also much larger than when using linear EDFs, and as $Pe^{*}_{\Delta x}$ increases, stable solutions will only be found for low Courant numbers.

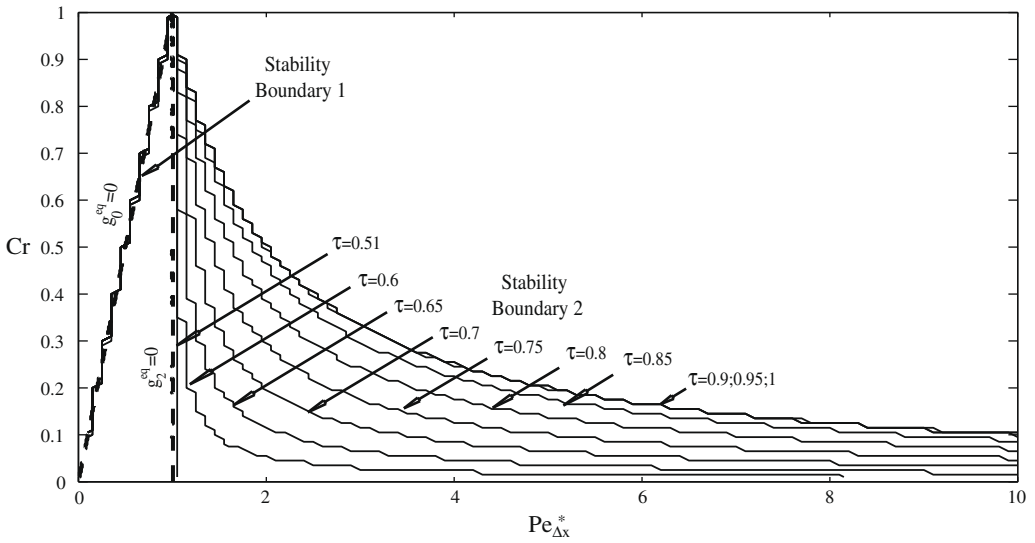

Fig. 5. Stability and non-negativity domains of D1Q3 lattice with linear EDFs. The stability domain is the area underneath the stability boundaries (solid lines). The non-negativity domain is the area underneath the non-negativity boundaries (dashed lines).

5.2. Stability analysis on D2Q9 and D2Q5

In this section, we analyze the LBGK stability for the D2Q9 and D2Q5 lattices. We first consider D2Q9. Since both lattices have symmetry with respect to the horizontal, vertical, and diagonal directions, we can reduce our study to the flow direction $\alpha \in [0, \pi/4]$, and any other directions will be equivalent to the one in this interval.

The procedure is the same as in the one-dimensional case, but **A** is a 9 by 9 matrix. In this problem, the angle α of the flow velocity with respect to the lattice grid will be an additional factor in the analysis. For different values of $\prod = (Pe^*_{\Delta x}, Cr, \tau, \alpha)$, the eigenvalues of the matrix **A** are calculated numerically. When solving the eigenvalue problem numerically in 2D, we use the dimensionless wave number $\beta_n = k_{mx} c_{jx} \Delta t$ and $\gamma_p = k_{my} c_{jy} \Delta t$. Then, $\exp(\mathbf{k}_m \cdot \mathbf{c}_j \Delta t) = \exp(\beta_n)\exp(\gamma_p)$, where $\beta_n = n2\pi/N$ and $\gamma_p = p2\pi/N$, and n and p go from 1 to N. N is the number of β_n and γ_p that we use.

Similar to the one-dimensional case, we test different values of the relaxation time, $\tau = 0.51$, 0.6, 0.7, 0.8, 0.9, and 1.0, to determine the stability domain. The number of the dimensionless wave numbers used is $N = 36$. The eigenvalue problem is solved twice based on the pairs $(Pe^*_{\Delta x}, Cr)$ and $(Pe_{\Delta x} Cr)$, using a grid of 100 by 100 points in each case.

The stability domains shown in Fig. 6 are for the D2Q9 lattice with second-order EDFs. For a specific flow direction $\alpha = 22.5°$ (Fig. 6(a) and (b)), the non-negativity domain shown in Fig. 6(a) is delineated using Eqs. (34) and (35). Fig. 6(a) shows growing stability domains based on $Pe^*_{\Delta x}$ and Cr as the relaxation time increases. Moreover, we can observe that the stability domain becomes the non-negativity domain when the relaxation time is very close to 0.5.

Similar to the one-dimensional case, given $(Pe^*_{\Delta x}, Cr, \alpha)$ in Fig. 6(a) there is a minimum value of the relaxation time for stable solutions. However, if $Pe_{\Delta x}$ is used, the stability boundaries for different values of relaxation time can intersect each other (Fig. 6(b)). Hence, given ($Pe_{\Delta x}$,Cr,α), increasing the relaxation time does not guarantee a stable solution in general.

Fig. 6(c) and (d) shows the domain resulting from the intersecting stability domains for five flow directions $\alpha = (i-1)\pi/16$, $i = 1, 2, \ldots, 5$. The non-negativity domain in Fig. 6(c) is also obtained by considering intersections of the non-negativity domains for those flow directions. Fig. 6(c) and (d) were obtained as an approximation to the stability domain for any direction of the flow, which would result from intersecting stability domains for $\forall \alpha \in [0, \pi/4]$.

Next, we consider the case of neglecting the second-order terms in the EDFs. It is noted that D2Q5 with linear EDFs can recover the same moments as D2Q9 with linear EDFs, and therefore the same macroscopic equation. This motivates our interest in comparing these two lattices.

Fig. 7 shows the non-negativity and stability domains using linear EDFs for the D2Q5 and D2Q9 lattices with the five flow directions $\alpha = (i-1)\pi/16$, $i = 1, 2, \ldots, 5$. The stability domains of the D2Q9 are slightly larger than those for D2Q5. However, the D2Q9 non-negativity domain is slightly smaller than that for the D2Q5 lattice.

Comparing Fig. 7 with Fig. 6, we observe that second-order EDFs give larger non-negativity and stability domains than those given by linear EDFs. Linear EDFs only offer stable solutions for low Courant numbers as $Pe^*_{\Delta x}$ increases, while second-order EDFs can produce stable solution at higher Courant numbers.

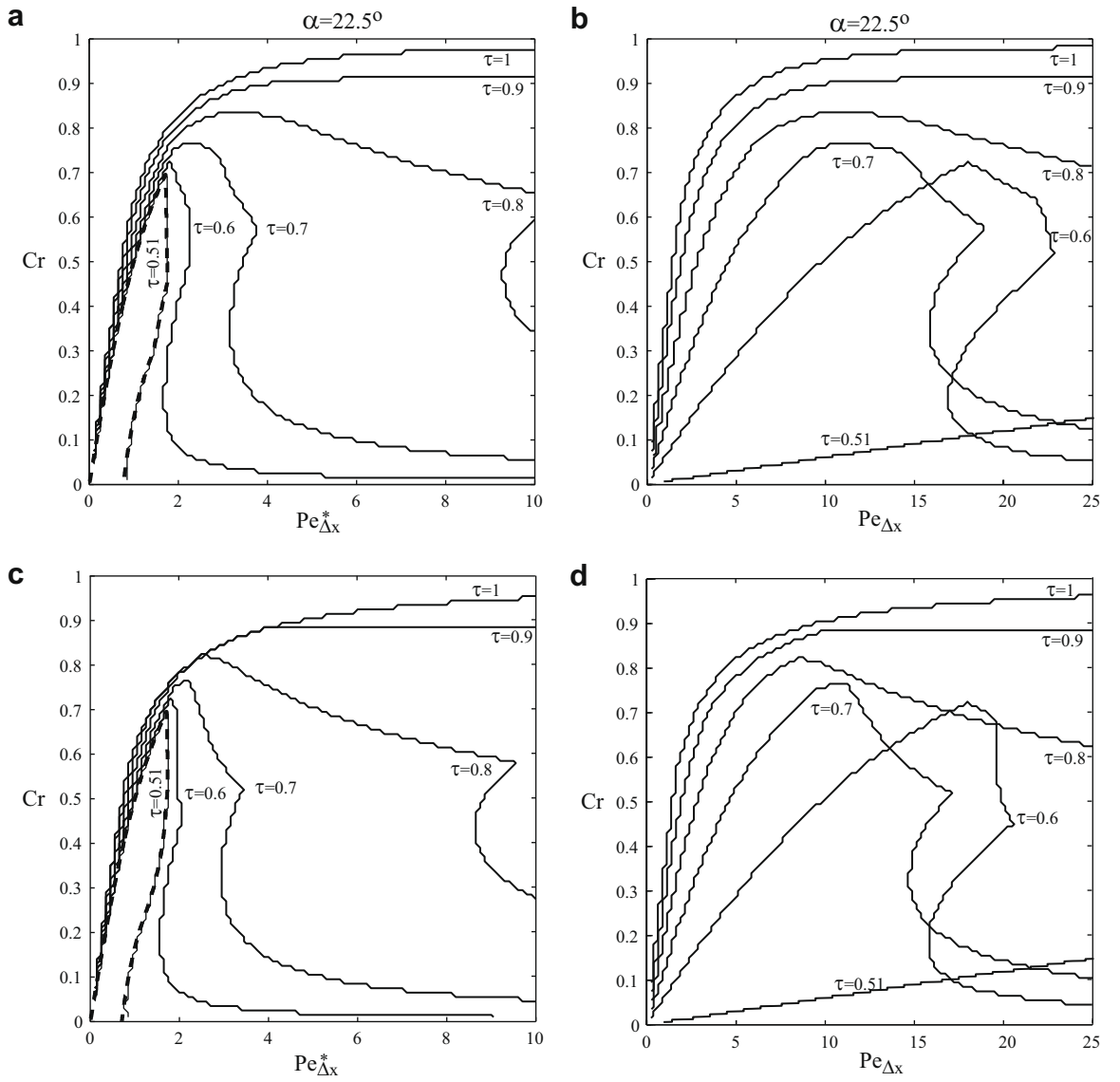

Fig. 6. Stability and non-negativity domains for D2Q9 lattice with second-order EDFs. (a) and (b) are for the specific case $\alpha = 22.5°$. (c) and (d) consider five flow directions ($\alpha = 0°$, 11.25°, 22.5°, 33.75°, and 45°) simultaneously. The stability domain is the area underneath the stability boundaries (solid lines). The non-negativity domain is the area underneath the non-negativity boundaries (dashed lines).

6. Numerical examples

6.1. One-dimensional mass transport in uniform flow

This section presents numerical experiments to demonstrate the stability problem of using the LBGK to solve the one-dimensional ADE. The governing equation for uniform flow is

$$\frac{\partial C}{\partial t} + U\frac{\partial C}{\partial x} = D\frac{\partial^2 C}{\partial x^2} \tag{53}$$

where C is the concentration of a substance, U is the velocity of the flow in the x direction, and D is the diffusion coefficient. We consider an infinite domain and the following initial condition:

$$C(x, t = 0) = \frac{1}{\sqrt{10\pi}} \exp\left(-\frac{x^2}{10}\right) \tag{54}$$

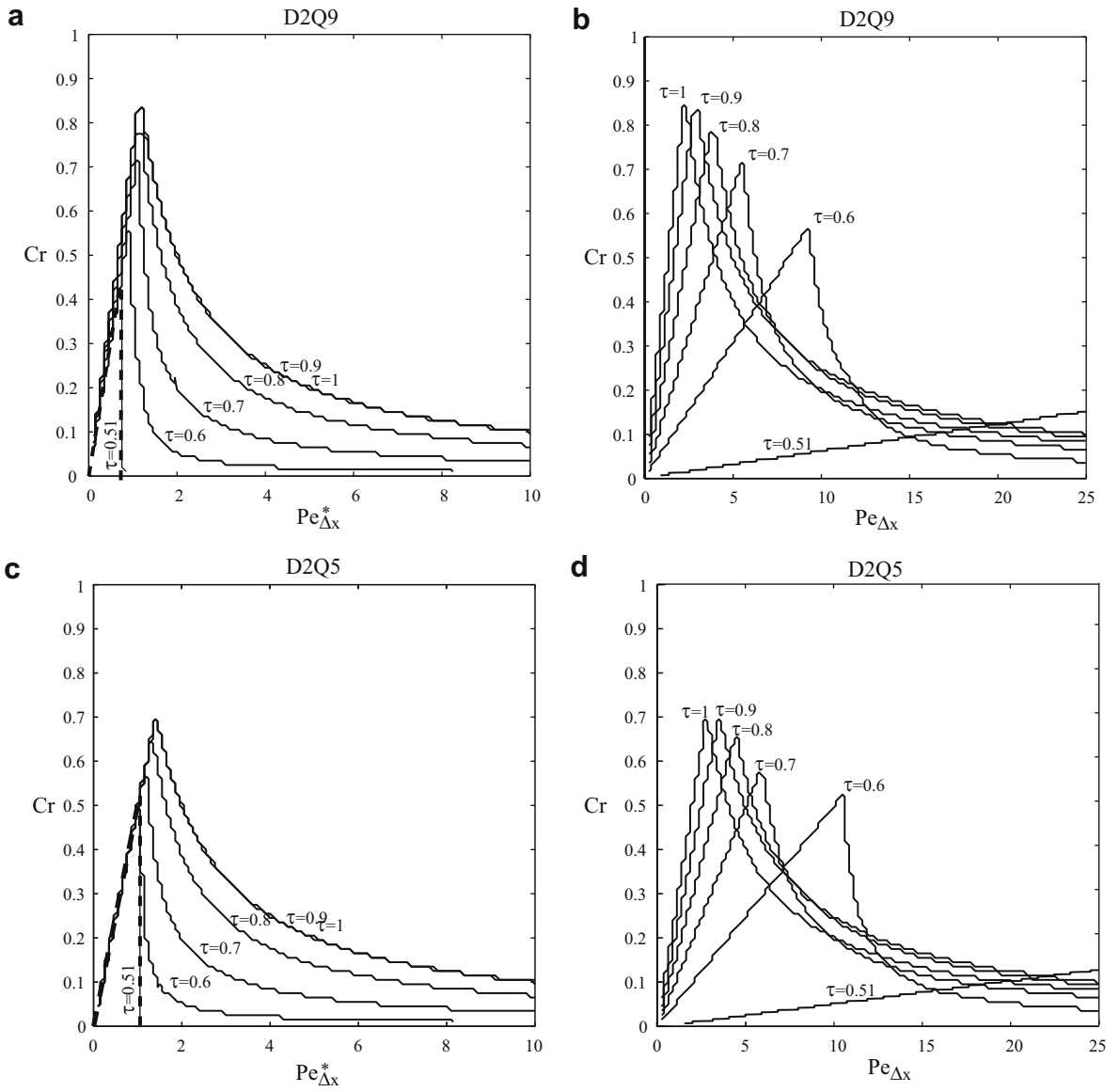

Fig. 7. Stability and non-negativity domains for D2Q9 and D2Q5 lattices with linear EDFs considering five flow directions ($\alpha = 0°$, 11.25°, 22.5°, 33.75°, and 45°) simultaneously. The stability domain is the area underneath the stability boundaries (solid lines). The non-negativity domain is the area underneath the non-negativity boundaries (dashed lines).

The exact solution for Eq. (53) with the initial condition Eq. (54) is

$$C(x,t) = \frac{1}{\sqrt{\pi(4Dt+10)}} \exp\left(-\frac{(x-Ut)^2}{4Dt+10}\right) \tag{55}$$

We use a lattice size $\Delta x = 1$ and time step $\Delta t = 1$ for all the simulations. The case study tests different values of $Pe_{\Delta x}$, Cr, and τ. Then, the velocity U and the diffusion coefficient D are obtained from the following relationships:

$$U = \frac{Cr\Delta x}{\Delta t} \tag{56}$$

$$D = \frac{U\Delta x}{Pe_{\Delta x}} = \frac{Cr\Delta x^2}{Pe_{\Delta x}\Delta t} \tag{57}$$

The initialization of the particle distribution functions is as follows:

$$f_i(x, t = 0) = f_i^{eq}(x, t = 0) = C(x, t = 0) g_i^{eq}. \quad (58)$$

In each time step, we calculate the deviation of the LBM solution from the analytical solution at each node, i.e., $\varepsilon_j^t = |C_a(x_j, t) - C_n(x_j, t)|$. Then, the total error at time t is obtained by summing the nodal error over the entire computational domain, i.e., $\varepsilon_T^t = \sum_j \varepsilon_j^t$. The computational domain is large enough to ensure that the concentrations at the extremes are very close to zero such that no significant error is introduced from the edges.

Fig. 8 shows the numerical results using second-order EDFs for the relaxation times $\tau = 0.51$, 0.6, 0.7, 0.8, 0.9, 1, 2, and 3 for $Pe_{\Delta x} = 50$ and $Cr = 0.8$. By running one thousand time steps, $\tau = 0.51$ and 0.7 provide unstable solutions, as we observe in Fig. 8(a). The unstable solutions are confirmed by Fig. 4, in which the pair $Pe_{\Delta x} = 50$ and $Cr = 0.8$ lie in the unstable domains for $\tau = 0.51$ and 0.7. On the other hand, the pair $Pe_{\Delta x} = 50$ and $Cr = 0.8$ gives the module of the eigenvalues of matrix **A** in Eq. (50) less than unity for $\tau = 0.6$, 0.8, 0.9, 1.0, 2.0, and 3.0 and results in stable solutions (Fig. 8(a)). The stability when $\tau = 0.6$, 0.8, 0.9, and 1.0 can be found in Fig. 4. Furthermore, the total errors for relaxation times larger than one greatly increase, indicating that much more numerical dispersion has been introduced.

None of the relaxation times considered in Fig. 8(a) makes the pair of $Pe_{\Delta x} = 50$ and $Cr = 0.8$ lie in the non-negativity domain except for $\tau = 0.6$. This confirms that using negative EDFs does not necessarily lead to unstable solutions.

Fig. 8(b) shows normalized concentration distributions after one thousand time steps. The simulated concentrations are normalized by dividing concentrations by the maximum value of the exact solution at that time, i.e., $C_{max}(t) =$

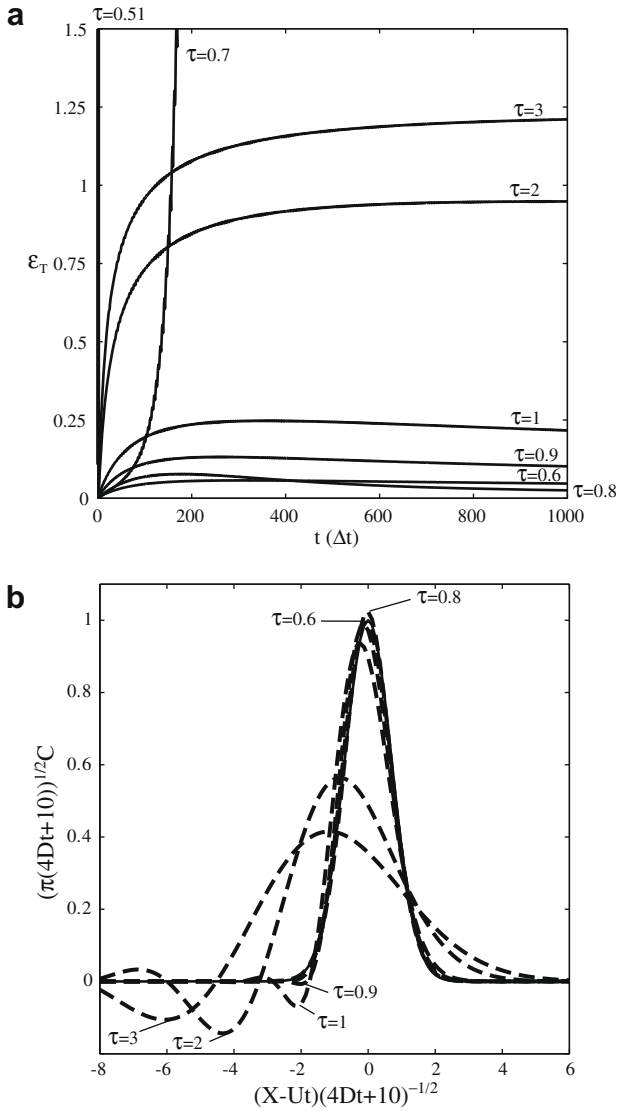

Fig. 8. (a) Evolution of total errors for 1,000 time steps with $Pe_{\Delta x} = 50$ and $Cr = 0.8$ using different τ values, 1D case. (b) Normalized concentration results against the exact solutions at 1000, time steps.

$1/\sqrt{\pi(4Dt+10)}$, and the normalized horizontal coordinate is obtained by $(x-Ut)/\sqrt{4Dt+10}$. After normalization, the exact solutions become space and time invariant.

Fig. 8(b) shows that numerical dispersion greatly increases for relaxation times larger than one, i.e., the greater the numerical dispersion, the greater the total error (Fig. 8(a)). Based on Fig. 8, we find that the most accurate solution is obtained for values of the relaxation time $\tau \approx 0.8$. However, selecting $\tau = 0.8$ does not always ensure stability.

Fig. 9 compares the total errors and solutions after 1000 time steps using linear and second-order EDFs for $Pe_{\Delta x} = 10$ and $Cr = 0.15$. None of the pairs of $Pe_{\Delta x} = 10$ and $Cr = 0.15$ using the τ values in Fig. 9 lies in the non-negativity domains of linear and second-order EDFs except for $\tau = 0.6$. The second-order EDFs produce more accurate solutions and have much less numerical dispersion than the linear EDFs. Moreover, when using linear EDFs the numerical dispersion increases as τ increases. On the other hand, second-order EDFs introduce the least numerical dispersion for $\tau = 0.8$.

Fig. 10 shows the results after 100,000 time steps for $Pe_{\Delta x} = 50$, $Cr = 0.05$, and $\tau = 0.9$ using second-order EDFs. Based on Fig. 4(b) this set of parameters indicates a stable solution. The stable solution is also confirmed in Fig. 10(a), where the total error gradually reaches a peak and then starts decreasing. This behavior distinguishes stable solutions from unstable solutions that exhibit exponentially increasing errors as shown in Fig. 8. Fig. 10(b) presents normalized concentrations at 10^3, 10^4, and 10^5 time steps against the exact solutions. The degree of dispersive behavior reflects the magnitude of total errors in Fig. 10(a).

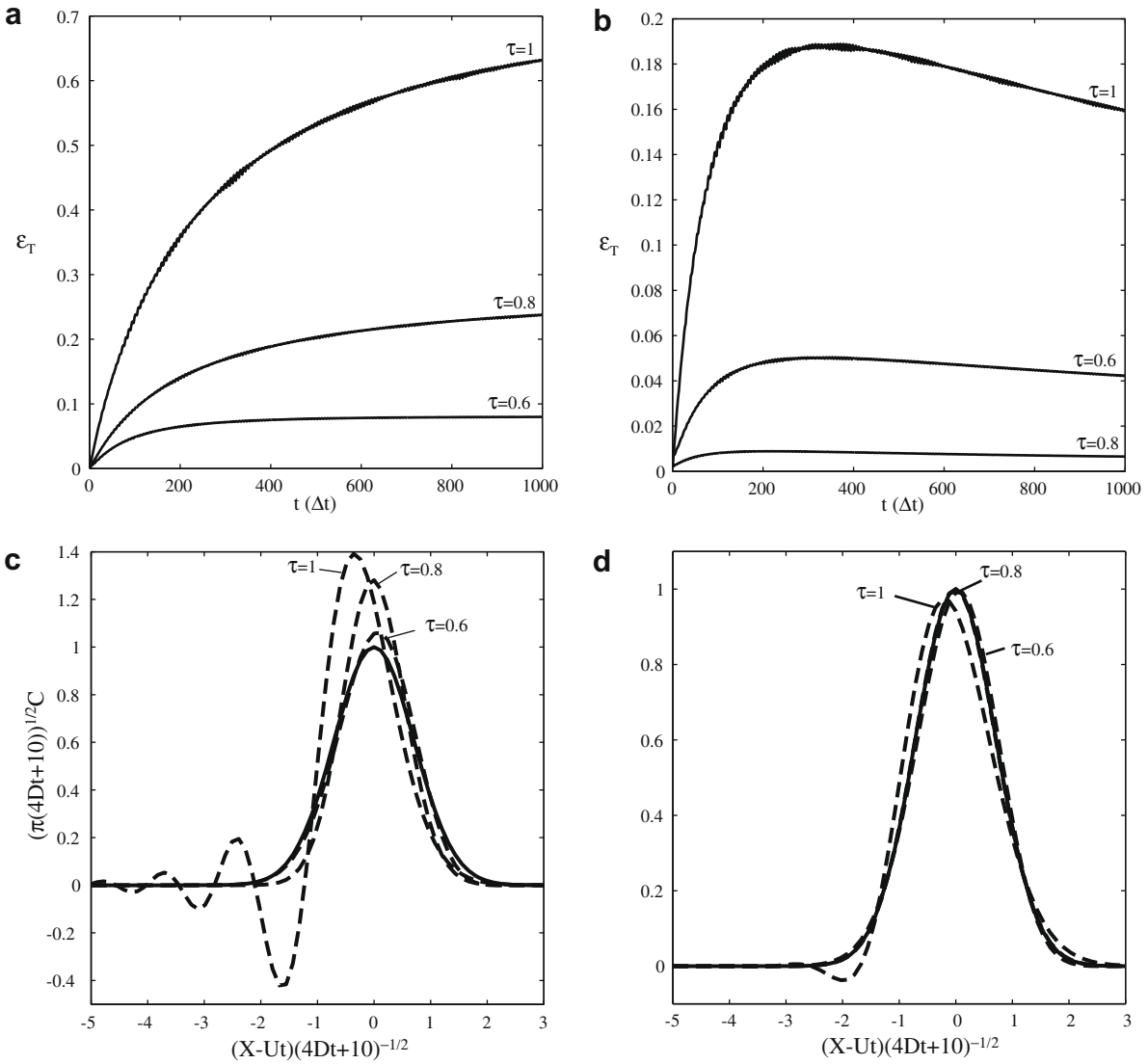

Fig. 9. Comparison between linear (figures (a) and (c)) and second-order (figures (b) and (d)) EDFs for 1D transport problem. $Pe_{\Delta x} = 10$ and $Cr = 0.15$. Figures (a) and (b): evolution of errors. Figures (c) and (d): normalized concentration distribution after 1000 time steps. LBM solutions (dashed lines); exact solution (solid lines).

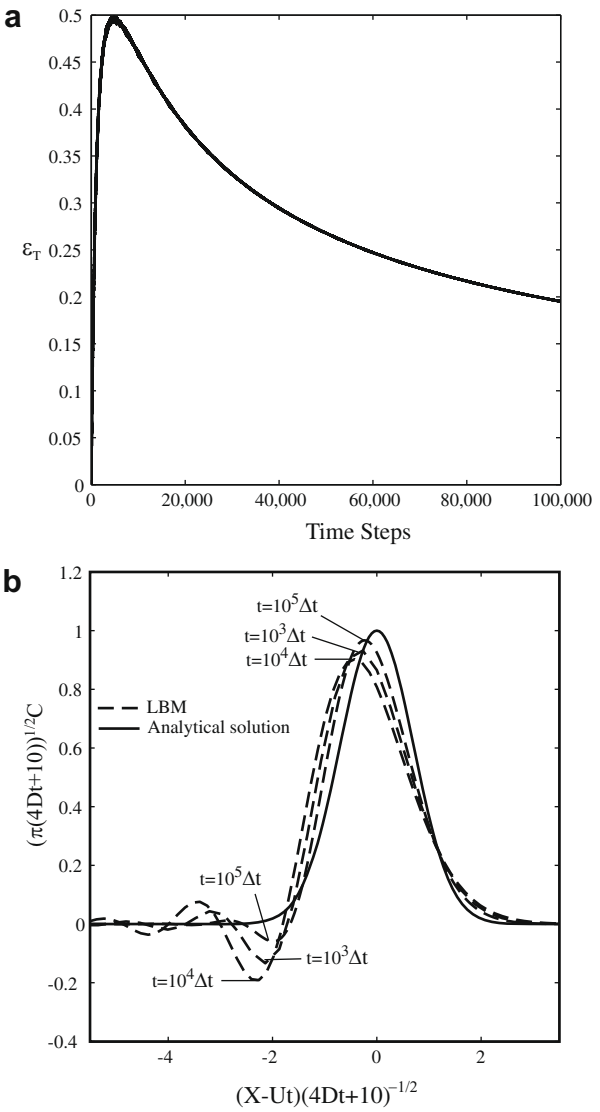

Fig. 10. (a) Evolution of total error for 100,000 time steps for $Pe_{\Delta x} = 50$, $Cr = 0.05$, and $\tau = 0.9$, 1D case. (b) Normalized concentrations at 1000, 10,000, and 100,000 time steps.

6.2. Two-dimensional mass transport in uniform flow

This case considers the mass transport of a conservative solute in a two-dimensional infinite domain. The flow field is considered uniform and constant. The initial condition is

$$C(x,y,t=0) = \frac{1}{10\pi}\exp\left(-\frac{x^2+y^2}{10}\right) \tag{59}$$

The exact solution for this problem with the initial condition Eq. (59) is

$$C(x,y,t) = \frac{1}{\pi(4Dt+10)}\exp\left(-\frac{(x-Ut)^2+(y-Vt)^2}{4Dt+10}\right) \tag{60}$$

where U and V are constant velocities along the x and y directions. The initialization of the particle distribution functions used is as follows:

$$f_i(x,y,t=0) = f_i^{eq}(x,y,t=0) = C(x,y,t=0)g_i^{eq} \tag{61}$$

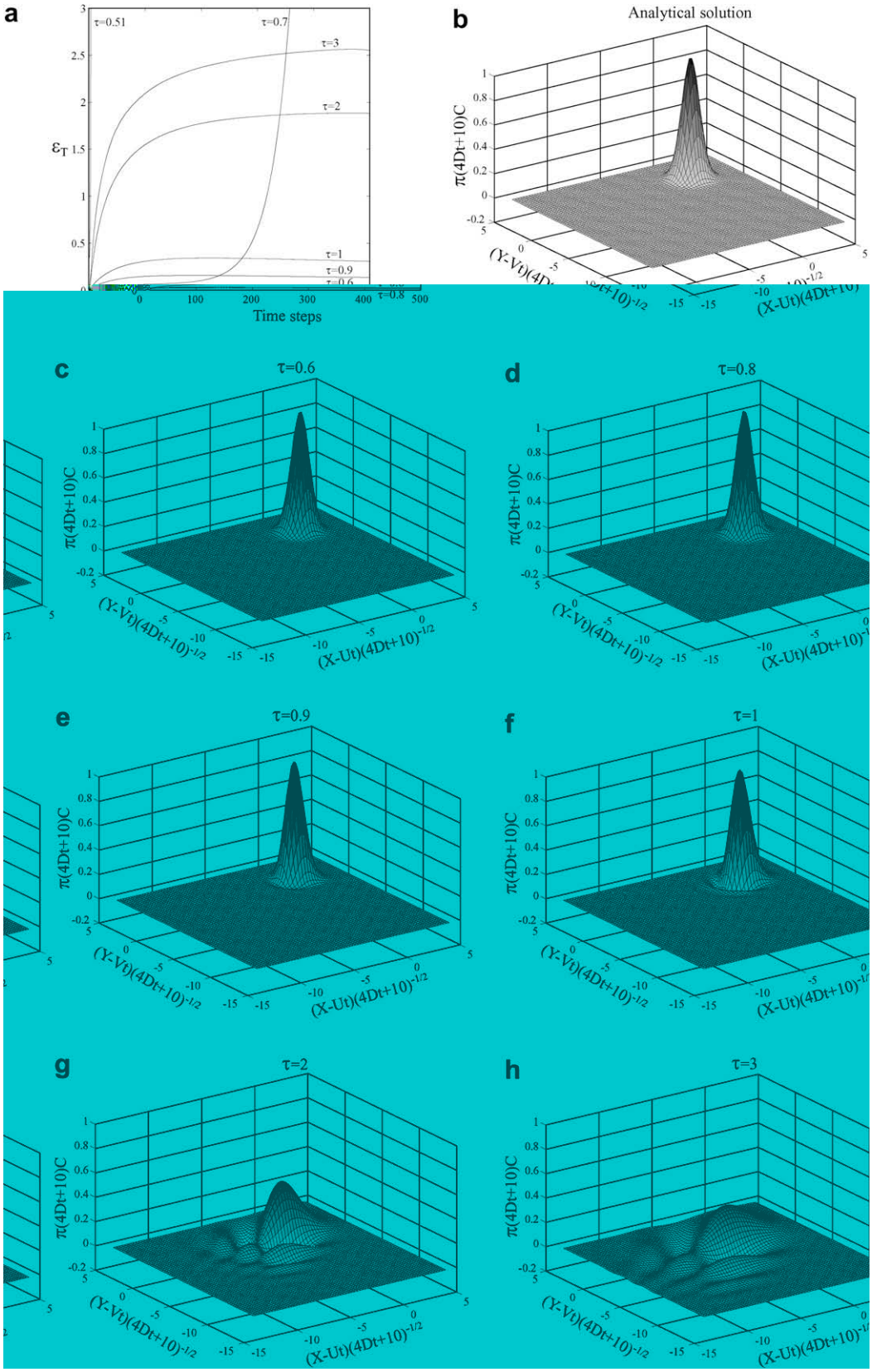

Fig. 11. (a) Evolution of total errors for $Pe_{\Delta x} = 20$, $Cr = 0.5$, and $\alpha = 22.5^\circ$ using D2Q9 with second-order EDFs; (b) analytic solution; (c)–(h) normalized concentration distributions after 500 time steps.

The total error is calculated as in the one-dimensional case. We use a square lattice with $\Delta x = \Delta y = 1$ and time step $\Delta t = 1$ for all the simulations. The second-order EDFs are considered. The case study is specified providing the values of $Pe_{\Delta x}$, Cr, and τ. Then, the velocity $\mathbf{u} = (U,V)$ is obtained from $|\mathbf{u}| = Cr\Delta x/\Delta t$, $U = |\mathbf{u}|\cos\alpha$, and $V = |\mathbf{u}|\sin\alpha$, and the diffusion coefficient D is obtained from Eq. (57).

This case tests the stability of the solutions with relaxation times $\tau = 0.51$, 0.6, 0.7, 0.8, 0.9, 1.0, 2.0, and 3.0 when $Pe_{\Delta x} = 20$, $Cr = 0.5$ and $\alpha = 22.5°$. None of these τ values places the pair $Pe_{\Delta x} = 20$ and $Cr = 0.5$ in the non-negativity domain. Fig. 6(b) implies stable solutions for $\tau = 0.6$, 0.8, 0.9, and 1.0, and unstable solutions for $\tau = 0.51$ and 0.7. Moreover, the module of the eigenvalue of the matrix $\mathbf{A}$ in Eq. (50) is less than unity for $\tau = 2$ and 3. The numerical results in Fig. 11 confirm these implications.

Fig. 11(a) shows the evolution of the total errors for each case up to 500 time steps. Unstable solutions for $\tau = 0.51$ and 0.7 are obvious. Fig. 11(b)–(h) shows the normalized concentration distribution after five hundred time steps for the analytical solution (Fig. 11(b)) and the LBM results (Fig. 11(c)–(h)). In this case, we observe that $\tau = 0.8$ provides the best solution, as occurred in the one-dimensional cases. Moreover, numerical dispersion increases when τ is larger than 0.8. While $\tau = 1$ produced a good solution with moderate numerical dispersion (Fig. 11(f)), using τ values larger than unity introduced too much numerical dispersion (Fig. 11(g) and (h)).

7. Conclusions

The dimensionless equilibrium distribution functions (EDFs) facilitate the non-negativity and linear stability analysis of the LBGK model by reducing variables to four collective parameters: the scaled Peclet number, the Courant number, the single relaxation time and the flow direction. Although dedicated to analyzing the advection–diffusion equation (ADE), the dimensionless EDFs are also applicable to delineating non-negativity and stability domains for hydrodynamics equations by shifting the parameters to Reynolds number and Mach number.

For a given set of parameters (scaled Peclet number, Courant number, and flow directions), there exists a minimum value of the relaxation time to determine stable solutions. Then, this set of parameters always produces stable solutions for any values of the relaxation time larger than this minimum value.

The linear stability domains were obtained for three different lattices with linear and second-order EDFs. In all cases, the linear stability domain covers the non-negativity domain. In other words, non-negativity of the dimensionless EDFs presents a sufficient condition for the linear stability of the LBGK, but is not a necessary condition since stable solutions can be obtained even if some EDF values are negative. Moreover, the non-negativity becomes a necessary condition when the relaxation time is very close to 0.5.

Second-order EDFs have larger stability domains than linear EDFs, which makes the LBGK more likely to be stable if second-order EDFs are employed. Furthermore, if both linear and second-order EDFs produce stable solutions using the same set of parameters, the second-order EDFs result in less numerical dispersion.

Acknowledgments

This research was supported in part by the Louisiana Board of Regents under award LEQSF (2005–08)-RD-A-12 and the Department of the Interior, US Geological Survey under Grant No. 05HQGR0142 and 06HQGR0088 through the Louisiana Water Resources Research Institute. The first author acknowledges Mutua Madrileña Automovilista for financial support. This work was greatly improved by the thorough, constructive reviews provided by two anonymous reviewers.

Appendix A. Non-negativity analysis for D1Q3, D2Q5, and D2Q9

A.1. D1Q3 lattice with linear EDFs

The linear dimensionless EDFs for D1Q3 lattice are

$$g_1^{eq} = \frac{1}{2}\left(\frac{Cr}{Pe_{\Delta x}^*} + Cr\cos\alpha\right) \tag{A.1}$$

$$g_2^{eq} = \frac{1}{2}\left(\frac{Cr}{Pe_{\Delta x}^*} - Cr\cos\alpha\right) \tag{A.2}$$

$$g_0^{eq} = 1 - \left(\frac{Cr}{Pe_{\Delta x}^*}\right) \tag{A.3}$$

where g_1^{eq} is the dimensionless EDFs for particles moving in the same direction of the flow, and g_2^{eq} is for particles moving in the opposite direction of the flow. $g_0^{eq} \geqslant 0$ results in $Pe_{\Delta x}^* - Cr \geqslant 0$; and $g_2^{eq} \geqslant 0$ results in $1 - Pe_{\Delta x}^* \geqslant 0$. Therefore, the non-negativity set is

$$S_L^{D1Q3} = \left\{ (Pe^*_{\Delta x}, Cr) \middle| \begin{matrix} Pe^*_{\Delta x} > 0, Cr > 0 \\ Pe^*_{\Delta x} - Cr \geqslant 0 \\ 1 - Pe^*_{\Delta x} \geqslant 0 \end{matrix} \right\} \tag{A.4}$$

A.2. D1Q3 lattice with second-order EDFs

The second-order dimensionless EDFs of D1Q3 lattice are

$$g_1^{eq} = \frac{1}{2}\left(\frac{Cr}{Pe^*_{\Delta x}} + Cr\cos\alpha + Cr^2\right) \tag{A.5}$$

$$g_2^{eq} = \frac{1}{2}\left(\frac{Cr}{Pe^*_{\Delta x}} - Cr\cos\alpha + Cr^2\right) \tag{A.6}$$

$$g_0^{eq} = 1 - \left(\frac{Cr}{Pe^*_{\Delta x}} + Cr^2\right) \tag{A.7}$$

$g_0^{eq} \geqslant 0$ results in $Pe^*_{\Delta x} - Cr - Pe^*_{\Delta x}Cr^2 \geqslant 0$; and $g_2^{eq} \geqslant 0$ results in $1 - Pe^*_{\Delta x} + Pe^*_{\Delta x}Cr \geqslant 0$. Therefore, the non-negativity set is

$$S_{NL}^{D1Q3} = \left\{ (Pe^*_{\Delta x}, Cr) \middle| \begin{matrix} Pe^*_{\Delta x} > 0, Cr > 0 \\ Pe^*_{\Delta x} - Cr - Pe^*_{\Delta x}Cr^2 \geqslant 0 \\ 1 - Pe^*_{\Delta x} + Pe^*_{\Delta x}Cr \geqslant 0 \end{matrix} \right\} \tag{A.8}$$

A.3. D2Q5 lattice with linear EDFs

For a given flow direction α, the linear dimensionless EDFs of D2Q5 lattice are

$$g_1^{eq} = \frac{1}{2}\left(\frac{Cr}{Pe^*_{\Delta x}} + Cr\cos\alpha\right) \tag{A.9}$$

$$g_2^{eq} = \frac{1}{2}\left(\frac{Cr}{Pe^*_{\Delta x}} + Cr\sin\alpha\right) \tag{A.10}$$

$$g_3^{eq} = \frac{1}{2}\left(\frac{Cr}{Pe^*_{\Delta x}} - Cr\cos\alpha\right) \tag{A.11}$$

$$g_4^{eq} = \frac{1}{2}\left(\frac{Cr}{Pe^*_{\Delta x}} - Cr\sin\alpha\right) \tag{A.12}$$

$$g_0^{eq} = \left(1 - 2\frac{Cr}{Pe^*_{\Delta x}}\right) \tag{A.13}$$

The following relationships stand for any $\alpha \in [0, \pi/4] : g_1^{eq} \geqslant g_3^{eq}, g_2^{eq} \geqslant g_4^{eq}$. Therefore,

$$S_{L\alpha}^{D2Q5} = \left\{ (Pe^*_{\Delta x}, Cr) \middle| \begin{matrix} Pe^*_{\Delta x} > 0, Cr > 0 \\ 1 - 2\frac{Cr}{Pe^*_{\Delta x}} \geqslant 0 \\ \frac{Cr}{Pe^*_{\Delta x}} - Cr\lambda_i \geqslant 0, i = 3, 4 \end{matrix} \right\} \tag{A.14}$$

where $\lambda_3 \in \left[\sqrt{2}/2, 1\right]$ and $\lambda_4 \in \left[0, \sqrt{2}/2\right]$. The non-negativity set is $S_L^{D2Q5} = \cap_{\alpha\in[0,\pi/4]} S_{L\alpha}^{D2Q5}$, which can be expressed as

$$S_L^{D2Q5} = \left\{ (Pe^*_{\Delta x}, Cr) \middle| \begin{matrix} Pe^*_{\Delta x} > 0, Cr > 0 \\ 1 - 2\frac{Cr}{Pe^*_{\Delta x}} \geqslant 0 \\ \frac{Cr}{Pe^*_{\Delta x}} - Cr\lambda \geqslant 0, \quad \forall\lambda \in [0, 1] \end{matrix} \right\} \tag{A.15}$$

which leads to

$$S_L^{D2Q5} = \left\{ (Pe^*_{\Delta x}, Cr) \middle| \begin{matrix} Pe^*_{\Delta x} > 0, Cr > 0 \\ Pe^*_{\Delta x} - 2Cr \geqslant 0 \\ Pe^*_{\Delta x} \leqslant 1 \end{matrix} \right\} \tag{A.16}$$

A.4. D2Q9 with linear EDFs

For a given flow direction α, the linear dimensionless EDFs of D2Q5 lattice are

$$g_1^{eq} = \frac{1}{3}\left(\frac{Cr}{Pe^*_{\Delta x}} + Cr\cos\alpha\right) \tag{A.17}$$

$$g_2^{eq} = \frac{1}{3}\left(\frac{Cr}{Pe^*_{\Delta x}} + Cr\sin\alpha\right) \tag{A.18}$$

$$g_3^{eq} = \frac{1}{3}\left(\frac{Cr}{Pe^*_{\Delta x}} - Cr\cos\alpha\right) \tag{A.19}$$

$$g_4^{eq} = \frac{1}{3}\left(\frac{Cr}{Pe^*_{\Delta x}} - Cr\sin\alpha\right) \tag{A.20}$$

$$g_6^{eq} = \frac{1}{12}\left(\frac{Cr}{Pe^*_{\Delta x}} + Cr(-\cos\alpha + \sin\alpha)\right) \tag{A.21}$$

$$g_7^{eq} = \frac{1}{12}\left(\frac{Cr}{Pe^*_{\Delta x}} - Cr(\cos\alpha + \sin\alpha)\right) \tag{A.22}$$

$$g_8^{eq} = \frac{1}{12}\left(\frac{Cr}{Pe^*_{\Delta x}} + Cr(\cos\alpha - \sin\alpha)\right) \tag{A.23}$$

$$g_0^{eq} = \left(1 - \frac{5}{3}\frac{Cr}{Pe^*_{\Delta x}}\right) \tag{A.24}$$

The following relationships $g_1^{eq} \geqslant g_3^{eq}$, $g_2^{eq} \geqslant g_4^{eq}$, $g_5^{eq} \geqslant g_7^{eq}$ and $g_8^{eq} \geqslant g_6^{eq}$ are valid for any $\alpha \in [0,\pi/4]$. Therefore, we have

$$S_{L\alpha}^{D2Q9} = \left\{ (Pe^*_{\Delta x}, Cr) \middle| \begin{array}{l} Pe^*_{\Delta x} > 0, Cr > 0 \\ 1 - \frac{5}{3}\frac{Cr}{Pe^*_{\Delta x}} \geqslant 0 \\ \frac{Cr}{Pe^*_{\Delta x}} - Cr\lambda_i \geqslant 0, \quad i = 3,4,6,7 \end{array} \right\} \tag{A.25}$$

The non-negativity set is $S_L^{D2Q9} = \cap_{\alpha\in[0,\pi/4]} S_{L\alpha}^{D2Q9}$, which can be expressed as:

$$S_L^{D2Q9} = \left\{ (Pe^*_{\Delta x}, Cr) \middle| \begin{array}{l} Pe^*_{\Delta x} > 0, Cr > 0 \\ 1 - \frac{5}{3}\frac{Cr}{Pe^*_{\Delta x}} \geqslant 0 \\ \frac{Cr}{Pe^*_{\Delta x}} - Cr\lambda \geqslant 0, \ \forall\lambda \in [0,\sqrt{2}] \end{array} \right\} \tag{A.26}$$

which leads to

$$S_L^{D2Q9} = \left\{ (Pe^*_{\Delta x}, Cr) \middle| \begin{array}{l} Pe^*_{\Delta x} > 0, Cr > 0 \\ 3Pe^*_{\Delta x} - 5Cr \geqslant 0 \\ Pe^*_{\Delta x} \leqslant \sqrt{2}/2 \end{array} \right\} \tag{A.27}$$

References

[1] S. Chen, G.D. Doolen, Lattice Boltzmann method for fluid flows, Annual Review of Fluid Mechanics 30 (1) (1998) 329–364.
[2] D.H. Rothman, S. Zaleski, Lattice-Gas Cellular Automata: Simple Models of Complex Hydrodynamics, Cambridge University Press, UK, 1997.
[3] S.P. Dawson, S. Chen, G.D. Doolen, Lattice Boltzmann computations for reaction–diffusion equations, Journal of Chemical Physics 98 (2) (1993) 1514–1523.
[4] J.Q. Deng, M.S. Ghidaoui, W.G. Gray, K. Xu, A Boltzmann-based mesoscopic model for contaminant transport in flow systems, Advances in Water Resources 24 (5) (2001) 531–550.
[5] M. Yoshino, T. Inamuro, Lattice Boltzmann Simulations for flow and heat/mass transfer problems in a three-dimensional porous structure, International Journal of Numerical Methods in Fluids 43 (2) (2003) 183–198.
[6] J. Wang, M. Wang, Z. Li, A lattice Boltzmann algorithm for fluid–solid conjugate heat transfer, International Journal of Thermal Sciences 46 (3) (2007) 228–234.
[7] P. Bhatnagar, E. P Gross, M.K. Krook, A model for collision processes in gases: small amplitude processes in charged and neutral one component systems, Physical Review 94 (3) (1954) 511–525.
[8] J.D. Sterling, S. Chen, Stability analysis of lattice Boltzmann methods, Journal of Computational Physics 123 (1996) 196–206.
[9] R.A. Worthing, J. Mozer, G. Seeley, Stability of lattice Boltzmann methods in hydrodynamics regimes, Physical Review E 56 (2) (1997) 2243–2253.
[10] I.V. Karlin, A.N. Gorban, S. Succi, V. Boffi, Maximum entropy principle for lattice kinetic equations, Physical Review Letters 81 (1) (1998) 4.
[11] I.V. Karlin, A. Ferrante, H.C. Otttinger, Perfect entropy functions of the lattice Boltzmann method, Europhysics Letters 47 (2) (1999) 182–188.

[12] S. Ansumali, I.V. Karlin, Single relaxation time model for entropic lattice Boltzmann methods, Physical Review E 65 (056312) (2002).
[13] B.M. Boghosian, J. Yepez, P.V. Coveney, A. Wagner, Entropic lattice Boltzmann Methods, Proceedings of the Royal Society: Mathematical, Physical and Engineering Sciences 457 (2007) (2000) 707–766.
[14] W.-A. Yong, L.-S. Luo, Nonexistence of H theorem for the athermal lattice Boltzmann models with polynomial equilibria, Physical Review E 67 (051105) (2003) 1–4.
[15] S.S. Chikatamarla, S. Ansumali, I.V. Karlin, Entropic lattice Boltzmann models for hydrodynamics in three dimensions, Physical Review Letters 97 (2006) 4.
[16] S. Ansumali, I.V. Karlin, Stabilization of the lattice Boltzmann method by the H theorem: a numerical test, Physical Review E 62 (6) (2000) 7999–8003.
[17] B.M. Boghosian, P. Love, J. Yepez, Entropic lattice-Boltzmann model for Burger's equation, Philosophical Transactions Royal Society of London A (362) (2004) 1691–1701.
[18] S.S. Chikatamarla, I.V. Karlin, Entropy and Galilean invariance of lattice Boltzmann theories, Physical Review Letters 97 (190601) (2006) 1–4.
[19] Y. Li, R. Shock, R. Zhang, H. Chen, Numerical study of flow past an impulsively started cylinder by the lattice-Boltzmann method, Journal of Fluid Mechanics 519 (2004) 273–300.
[20] F. Tosi, S. Ubertini, S. Succi, H. Chen, I.V. Karlin, Numerical stability of entropic versus positivity-enforcing lattice Boltzmann schemes, Mathematics and Computers in Simulation 72 (2006) 227–231.
[21] R.A. Brownlee, A.N. Gorban, J. Levesley, Stabilization of the lattice Boltzmann method using the Ehrenfests' coarse-graining idea, Physical Review E 74 (037703) (2006) 1–4.
[22] R.A. Brownlee, A.N. Gorban, J. Levesley, Nonequilibrium entropy limiters in lattice Boltzmann methods, Physica A 387, 385–406.
[23] P. Lallemand, L.-S. Luo, Theory of the lattice Boltzmann method: dispersion, dissipation, isotropy, Galilean invariance and stability, Physical Review E 61 (6) (2000) 6546–6562.
[24] M.E. McCracken, J. Abraham, Multiple-relaxation-time lattice-Boltzmann model for multiphase flow, Physical Review E 71 (036701) (2005).
[25] I. Ginzburgh, Equilibrium-type and link-type lattice Boltzmann models for generic advection and anisotropic-dispersion equation, Advances in Water Resources 28 (11) (2005) 1171–1195.
[26] D.A. Wolf-Gladrow, Lattice-Gas Cellular Automata and Lattice Boltzmann Models: An Introduction, Springer, Berlin/Heidelberg, 2000.
[27] H. Yu, K. Zhao, Lattice Boltzmann method for compressible flows with high Mach numbers, Physical Review E 61 (4) (2000) 3867–3870.
[28] S. Suga, Numerical schemes obtained from lattice Boltzmann equations for advection diffusion equations, International Journal of Modern Physics C 17 (11) (2006) 1563–1577.
[29] X. He, X. Shan, G.D. Doolen, Discrete Boltzmann equation model for nonideal gases, Physical Review E 57 (1) (1998) R13–R16.
[30] E.G. Flekkøy, Lattice Bathnagar–Gross–Krook models for miscible fluids, Physical Review E 47 (6) (1993) 4247–4257.
[31] T. Inamuro, M. Yoshino, H. Inoue, R. Mizuno, F. Ogino, A lattice Boltzmann method for a binary miscible fluid mixture and its application to a heat-transfer problem, Journal of Computational Physics 179 (1) (2002) 201–215.
[32] I.V. Karlin, S. Ansumali, C.E. Frouzakis, S.S. Chikatamarla, Elements of the lattice Boltzmann Method: linear advection equation, Communications in Computational Physics 1 (2006) 616–655.